

# NUCLEAR ACTIVITY IN ISOLATED GALAXIES

Francisco J. Hernández-Ibarra<sup>1</sup>, Deborah Dultzin<sup>1</sup>, Yair Krongold<sup>1</sup>

<sup>1</sup>Instituto de Astronomía, Universidad Nacional Autónoma de México, Apartado Postal  
70-264, 04510 México DF, México.

Ascensión Del Olmo<sup>2</sup>, Jaime Perea<sup>2</sup> & J. J. González<sup>1</sup>

<sup>2</sup>Instituto de Astrofísica de Andalucía (C.S.I.C.) Apartado 3004, 18080 Granada, Spain

`hibarra@astro.unam.mx`

Received \_\_\_\_\_; accepted \_\_\_\_\_

Not to appear in Nonlearned J., 45.

## ABSTRACT

We present a spectroscopic study of the incidence of AGN nuclear activity in two samples of isolated galaxies (Karachentseva, V.E. & Varela, J.). Our results show that the incidence of non-thermal nuclear activity is about 43% and 31% for galaxies with emission lines and for the total sample 40% and 27% respectively. For the first time we have a large number of bona-fide isolated galaxies (513 objects), with statistically significant number of all morphological types. A large fraction ( $\sim 70\%$ ) of elliptical galaxies or early type spirals have an active galactic nucleus and  $\sim 70\%$  of them are LINERs. **We find a larger fraction of AGN in early morphological types, as also found in the general population of galaxies.** Only 3% of the AGN show the presence of broad lines (not a single one can be classified as type 1 AGN). This is a remarkable result which is at odds with the unified model even if we consider warped or clumpy tori. Finally, we interpret the large fraction of AGN in isolated galaxies as the result of **secular accretion.**

*Subject headings:* Galaxies: active - Galaxies: bulges - Galaxies: evolution - Galaxies: formation

## 1. Introduction

Along the last 25 years, many authors have studied the AGN environment (Stauffer 1982a,b; Dahari 1984, 1985; Kennicutt & Keel 1984; de Mello et al. 1995, 1996; Laurikainen & Salo 1995; Dultzin-Hacyan et al. 1999; Krongold et al. 2001, 2002; Schmitt 2001; Sorrentino et al. 2006; Koulouridis et al. 2006a,b; Márquez & Masegosa 2008). The incidence of nuclear activity in galaxies and their environment has become a topic of debate because there are different mechanisms that can possibly trigger nuclear activity depending on the galaxy’s environment. Interactions between galaxies are well known to produce enhancement in star formation in galaxies (Lonsdale et al. 1984; Kennicutt et al. 1987; Keel 1993; Krongold et al. 2002; Barton et al. 2000; Woods & Geller 2007; Lin et al. 2007). Others authors also have evidence for a connection between circumnuclear starburst and AGN (Storchi-Bergmann 2008, and references therein). There are also suggestions for a connection between interactions and nuclear non-thermal activity specifically of type 2 (Dultzin-Hacyan et al. 1999; Krongold et al. 2001). Other studies have dealt with the AGN population of compact groups (Martínez et al. 2010) as well as in larger groups.

The purpose of this project is to investigate the conditions to trigger AGN activity in different environments. In this paper we study the incidence of activity in isolated galaxies. In a forthcoming paper (Hernández-Ibarra et al. in preparation 2013) we will present the results of a survey of AGN in paired galaxies of similar mass.

It is important to study galaxies in a restricted environment in order to elucidate what mechanisms could be determinant to trigger AGN activity. Isolated galaxies can be defined as those systems that are formed in low galactic density environments, but that evolved without major interactions with other galaxies of not only similar mass over the last 3 Gyr. In this context, any non-axisymmetric structures in these galaxies such as bars, tails, plumes or stripping material must be the result of secular evolution.

The study of truly isolated galaxies is thus fundamental to benchmark the role of interactions in nuclear activity. Studies of field galaxies (e.g. Ho et al. 1997) cannot provide this information as these samples may include galaxies that have undergone or are undergoing an interaction.

**This is the first paper of a series involving a self consistent and homogeneous way to study nuclear activity in galaxies in different environments.** In the present work, we study the incidence of nuclear activity in two samples of bona-fide isolated galaxies using an efficient way to extract the stellar contribution (host spectrum). The purpose of this work is to have a well defined sample of isolated galaxies with optical spectroscopic characteristics that allow us to classify them according to their type of activity. **Studying the incidence of the nuclear activity in isolated galaxies alone is of great value to establish if AGN is a common and/or persistent phenomenon even when strong tidal external perturbations have not been present during the last few Gyr of galaxy evolution. This would indicate that AGN activity can be triggered by secular evolution processes in galaxies. Our results on this sample will be further used as a benchmark to compare the incidence of activity in a sample of isolated pair of galaxies (Hernández-Ibarra et al. in preparation 2013). Our samples of isolated and paired galaxies have been chosen to have consistent properties with each other except for the presence of a companion.**

This paper is organized as follows. In §2 we describe our samples. In §3 we present the data analysis and classification. Results are given in §4 and §5 contains the discussion about the possible mechanisms for developing an AGN in isolated galaxies.

## 2. Characteristics of the Samples

As stated above the so called “field galaxies” cannot be used as a proper sample in the study of the properties of truly isolated galaxies. Therefore in this study we used two samples of rigorously defined isolated galaxies: The photometric catalog of isolated galaxies (CIG) by Karachentseva (1973) and the northern isolated disk galaxies compiled by Varela et al. (2004).

We take all available spectra from DR7 of SDSS (Abazajian et al. 2009) for the two samples. The spectra have a wavelength coverage from 3800-9200Å with a resolution power of 1800-2200 and a signal-noise (S/N)  $>4$  per pixel at  $g=20.2$ . The SDSS spectra were taken through a fiber aperture of 3 arcsec in diameter (corresponding to 700 pc radii in average for our samples). This means only that central regions of the galaxies were observed.

The (CIG) catalog contains 1051 galaxies. It is one of the best sources of isolated objects. The isolation criteria are still used as the basis for new catalogs of isolated galaxies (e.g. Verdes-Montenegro et al. (2005); Karachentseva et al. (2010); Hernández-Toledo et al. (2010); Coziol et al. (2011); Karachentsev et al. (2011)). These isolation criteria guarantee that the galaxies have not experienced a major merger/interaction over the last 3 Gyr.

The catalog was based on a visual search of northern-sky galaxies ( $\delta \geq -3^\circ$ ) with a magnitude limit of  $m_{Zw} \leq 15.7$  and a range in  $z$  from  $\sim 0.01$  to  $0.05$ . Only objects **which have** high galactic latitude are considered in order to avoid galactic extinction<sup>1</sup> This sample, is reasonably complete ( $\sim 90\%$ ) in the magnitude range  $13.5 \leq m_{Zw} \leq 15.7$

---

<sup>1</sup>We know that our results are insensitive to reddening because we use line emission ratios which cancel this effect.

(Hernández Toledo et al. 1999). In this catalog a galaxy is considered to be isolated when it does not have a neighbor of similar size (diameter  $> \frac{1}{4}$  of the target galaxy) within 20 diameters. This corresponds to a magnitude difference  $\sim 3$  (excluding any possible AGN luminosity contamination). Considering a “field” velocity of 150 km/s for a galaxy with diameter of 25 kpc, it would require  $\sim 3$  Gigayears for a companion galaxy to abandon the area enclosed in the 20 diameters of isolation criterion. A similar time would be required to erase morphological perturbations due to a merger. This means that these galaxies have been unperturbed on average by at least that time.

The second sample we examined is that of northern isolated disk galaxies compiled by Varela et al. (2004) which originally contains 203 disk galaxies. This sample considers different criteria for isolation. In particular, it is based on the logarithmic ratio  $f$ , between inner and tidal forces acting upon the candidate galaxy by a possible perturber (see Varela et al. 2004, equation 3). Only galaxies with low  $f$  ratio ( $f \leq -4.5$ ) are considered as isolated because they do not show signatures of any perturbation. They estimated that the objects in their sample have not been affected by other galaxies during the last 2 Gyr. It is important sample obtained with different criteria to assess the reliability of our results.

We analyzed 413 spectra for the CIG catalog and 100 for Varela’s sample from SDSS DR7. After a meticulous inspection of the SLOAN images, we excluded those spectra which: 1) Do not have the optic fiber in the center of the galaxy (KIG 479 and KIG 237) or incomplete spectra like in KIG 702 and KIG 479, 2) Are Blue Compact/H II Galaxies (6 galaxies in Varela’s sample, 1 in CIG), 3) Galaxies showing traces of interaction (tidal tails etc) or present a companion namely: KIG 349, KIG 439, KIG 468, KIG 634 and KIG 687

(Sulentic et al. 2006; Verley et al. 2007) and 4) Galaxies that did not achieve  $3\sigma$  detection in all their line intensities (37 galaxies of CIG sample).

**A visual inspection was performed for all galaxies to confirm the morphological classification according to NED, SIMBAB and HYPERLEDA. In those few cases where an obvious misclassification was present, the morphology was corrected by us.** In addition we found that PGC 33255 could be part of a pair and excluded this galaxy of the sample. Strangely enough, we found two elliptical galaxies with a very blue compact core: PGC29177 and PGC43121 that show typical HII region spectra, and were also excluded from our analysis. With this into account, our spectroscopic sample from CIG consists of 367 galaxies while the spectroscopic sample from Varela consists of 93. Out of these galaxies 18 and 10 respectively do not present emission lines. In Table 1 we show the general statistics for both samples.

We were careful to distinguish between intrinsic no emission and a problem of detectability related to low S/N. For this purpose we set a threshold of  $10^{38}$  erg s<sup>-1</sup> in H $\alpha$  luminosity. The galaxies below this threshold are the true no-emission objects with a probability of being an AGN of less than 2% and 4% for the CIG and Varela’s samples respectively. The distribution of morphology and H $\alpha$  luminosity of our samples are presented in Figure 1.

### 3. Data Analysis and Nuclear Classification

We examined all of the spectra looking if emission lines were present. Within the spectral range covered by the SDSS spectra we searched for H $\beta$ , [OIII] $\lambda$ 5007Å, [OI] $\lambda$ 6300Å, [NII] $\lambda$ 6548,6584Å, H $\alpha$  and the two Sulfur ([SII] $\lambda$ 6717,6731Å) lines. In many cases the nebular emission is very weak or it can be even diluted in the strong stellar continuum of

the galaxy. Since the integrated SDSS spectra are collected through 3 arcsecs fibers, they include not only the nuclear emissions but also the surrounding stellar light coming from the host galaxy. This contamination turns out to be more significant at the central parts of the galaxies and as the spheroidal/bulge component becomes more relevant. In fact it can even mask weak emission lines such as those detected in galaxies with an AGN. Therefore to obtain a reliable nuclear classification based on the emission lines it is mandatory to subtract the stellar contribution. We applied the principal component analysis (PCA) method following Hao et al. (2005) to subtract this contribution. We used their first 8 eigenspectra from their low redshift range. These eigenspectra are the resulting eigenvectors of a PCA analysis applied to a sample of high S/N spectra of non-emission galaxies. In addition, as they pointed out, we included two more components, an A star spectrum accounting for the possible presence of post-starburst features and a power-law to take into account of the possible existence of a non-thermal component. The analysis is performed for all the spectra of our sample and it consists on a multiple regression of each spectrum to a linear combination of the 8 eigenspectra plus the two additional components. Previously to the fit each galaxy spectrum was moved to zero redshift which is the one of the template library. We also masked all those regions where emission lines may appear since the quality of the fit lies on the matching of the continua. Once the regression is performed, the direct subtraction of the resulting fit to the original ( $z=0$ ) spectrum provides us with a pure emission line spectrum where all the underlying absorption components and eventually a non thermal component of the continuum are removed.

**Line fluxes were calculated with Sherpa software (<http://cxc.cfa.harvard.edu/sherpa/>) (which comes in the CIAO distribution, <http://cxc.harvard.edu/ciao/>). Sherpa reads the data and evaluates a given model on this data set. Then, it varies the free parameters to minimize a statistical goodness function to obtain the best set of parameters that fit the data. In our case our model is composed only**



by Gaussians. The width and velocity of all the detected lines was constrained to the same value in our fits. Therefore we have as free parameters these two quantities and measured the intensity of each emission line. For those objects where a broad component was required in addition to the narrow one, an individual broad Gaussian was fitted with fully independent free parameters (see Figure 2 for fit examples).

We have used the Baldwin, Phillips and Terlevich optical diagnostic diagrams (Baldwin et al. 1981; Veilleux & Osterbrock 1987) to separate star-forming galaxies from active galactic nuclei (AGN). Line ratios adopted were  $([\text{O III}]/\text{H}\beta)$ ,  $([\text{N II}]/\text{H}\alpha)$ ,  $([\text{S II}]/\text{H}\alpha)$  and  $([\text{O I}]/\text{H}\alpha)$ . With these ratios we produced the  $([\text{O III}]/\text{H}\beta)$  vs  $([\text{N II}]/\text{H}\alpha)$  diagram (hereafter [N II] diagram), the  $([\text{O III}]/\text{H}\beta)$  vs  $([\text{S II}]/\text{H}\alpha)$  [S II] diagram and the  $([\text{O III}]/\text{H}\beta)$  vs  $([\text{O I}]/\text{H}\alpha)$  [O I] diagram. Line ratios with their errors and AGN type are presented in Tables 6 and 7 for CIG and Varela’s samples respectively. **The last column in these tables gives the nuclear type. We have used the quantitative definition by Winkler (1992) to measure the contribution of a broad component when present, and thus establish the Seyfert type.**

We used two demarcations to identify the galaxy type. The first one is the theoretical division line proposed by Kewley et al. (2001) (K01 line hereafter) where objects above this line on the diagrams have nuclear activity. The second one is the empirical line derived by Kauffmann et al. (2003a) (K03 line hereafter), this empirical line is based on the location of star-forming galaxies for the SDSS. Galaxies that lie between this two lines are called composite (or transition) objects. This objects need non-thermal processes to produce the line ratios (in addition to star forming processes). Therefore, we will take these objects as AGN in this work. Further support comes from the work done by Trouille et al. (2011) where they found that composite galaxies on BPT [N II] diagram are X-ray hard sources

and have a high X-ray luminosity to total infrared luminosity.

We have performed the analysis of the CIG catalog studying the effects of galactic morphology. Figure 3 shows a histogram of morphological types for both samples. It is clear that around 70 % of the galaxies in the CIG have morphologies between Sb and Sc. This result is consistent with a work done by Hernández-Toledo et al. (2010) for other isolated galaxy sample. The fraction of AGN for each morphological type in both samples is shown in Figure 4. We can see that within the large statistical errors the comparison is valid.

#### 4. Results

Our main results are summarized in Tables 2 to 5, and also in Figures 4 to 8.

In Table 2 we show numbers and percentages of activity and morphological classes for the CIG sample. Column 1 presents the morphological type, the total number of galaxies is listed in column 2. Columns 3 and 4 list the number of galaxies with H II and Composite (hereafter Comp) activity and their percentages, respectively. Column 5 contains the number of galaxies in the AGN+Comp region and their percentages. In column 6 we present the total number of galaxies including those with no-emission lines. Columns 7, 8 and 9 show the number and percentages for H II, Comp and AGN+Comp activity respectively. In Table 3 we present the same data as in Table 2 for Varela’s sample.

In Figure 5 we show the [N II] BPT diagram. All galaxies in the composite region are taken as AGN as argued in §3.

We can clearly see that the incidence of nuclear activity is statistically higher in early type galaxies and decreases gradually as we go to late types in this subsample of emission lines galaxies only. The dependence on morphology is quite significant: going from 70 % in E galaxies to 10 % in Sm. The incidence of nuclear starburst activity decreases in the

opposite sense: going from 90 % for Sm to 30 % for E. Meanwhile, if we consider the total sample (including galaxies without emission lines) the incidence gives a flatter distribution from E to Sb and decreases only for late types (compare columns 5 and 9 in Tables 2 and 3). This is clearly observed in Figure 4.

In Figure 6, we show the position of our objects in the BPT [N II] diagram for Varela’s sample. In this sample there are only 4 ellipticals, whereas the majority (27) are Sc. Considering that early types have a larger incidence of AGN, this can explain the fact that we find a total incidence of AGN of only 31 % as compared to 43 % in the CIG sample.

In Figure 7 we present the [S II] diagnostic diagram for the CIG sample. This diagram is useful to separate between Seyferts and LINERs.

In Figure 8. We show yet another diagram [O I]. This diagram differs only slightly from the one in Figure 7. The main difference is in the relative proportion of Seyferts and LINERS except for ellipticals. We point out that the [O I] line is weaker than the [S II] line and thus the mean error is large.

In Table 4. We quantify the incidence of AGN activity and morphology distribution derived from the [S II] and [O I] diagrams for CIG sample. Columns 1 and 2 are the morphological type and the number of galaxies in each type. In column 3 we list the number of AGN and the percentage in parentheses. The number of Seyfert galaxies and the percentage are listed in column 4. The number of LINERs is in column 5. Columns from 6 to 9 contains the same data of columns of 2 to 5 but this time for the [O I] diagram. Table 5 is the analogous of Table 4 for Varela’s sample.

**From these Tables we can confirm the result that the incidence of AGN activity is higher for early type galaxies in the sample with emission lines only. When all galaxies are considered the distribution flattens as found before for**

the CIG sample (see Fig.4). Again, the incidence of Seyfert galaxies is more frequent in morphologies from Sa to Sc, but specially in Sb.

In Tables 4 and 5 we show the data for the [S II] and [O I] diagrams. The AGN fractions are different from those in Tables 2 and 3. The reason is that we do not consider composite nuclei in the [S II] and [O I] diagrams. Unfortunately models by Kauffmann et al. (2003a) for these particular diagnostic diagrams ([S II] and [O I]) are not available. In consequence we only take into account the AGN activity with the Kewley limit for self-consistency.

We want to point out to recent models developed by Stasińska et al. (2006). These models predict lower values for the ratios of [N II]/H $\alpha$  and [O III]/H $\beta$  for AGN. In a Figure analogous to Fig. 5 the models by Stasińska et al. (2006) would produce an even larger zone of composite objects.

The most remarkable result is the absence of type 1 AGN for both samples. In the CIG sample there are 12 galaxies which show lines with a broad component. Five of these galaxies (all of them classified as Seyfert nuclei) have a clear broad component, three are Sy 1.5 (KIG 214, KIG 747, KIG 1008), one is Sy 1.8 (KIG 749) and one is Sy 1.9 (KIG 349). Other three objects (KIG 204, KIG 603 and KIG 605) are classified as LINERs. For two additional AGN (KIG 553, KIG 591) a Seyfert/LINER classification was not possible. The remaining two objects are HII galaxies with broad components. Broad components in HII regions are rare but have indeed been found (e.g. Binette et al. 2009).

In Varela's sample there is only one 1.8 type Seyfert galaxy (PGC48521). This object was classified as Sy 1 in SIMBAB and Sy 1.9 in NED. It has been shown that a few galaxies can vary their type with time (e.g. Shapovalova et al. 2008, 2012). Whether this is the case, or this object was misclassified in

SIMBAD has little relevance for our general conclusions.

To be conservative, we consider these 13 galaxies as the fraction of possible AGN with broad components (including the two HII galaxies to allow for any possible misclassification). These numbers indicate that the fraction of type 1 objects is  $\lesssim 3\%$ .

## 5. Discussion

The large number of galaxies of all morphological types permits us to quantify the link between morphology and nuclear activity. Our results indicate a close link between these two properties. This implies that any result of the incidence of activity without this consideration reflects the particular morphological distribution of the sample and therefore is not reliable. Our sample includes for the first time a statistically significant number of isolated early type galaxies (E+S0).

We found that Elliptical and SO galaxies have the highest incidence of nuclear activity in isolated environments when only galaxies with emission lines are considered (a similar result was found by Varela et al. (2004); Coziol et al. (2011); Sabater et al. (2012)). However, when the total sample is taken into account (including galaxies without emission lines) these apparent excess disappears and all early types (including Sa and Sb types) have similar fractions (see Fig. 4). This important difference could be found thanks to the large number of elliptical and spheroidal galaxies in our sample. This results are consistent with those found for “field” galaxies (Heckman 1980a; Keel 1983; Kauffmann et al. 2003a; Miller et al. 2003). Finding the same trend between isolated and field galaxies could be expected if we consider that AGN require

SMBHs and black holes are correlated with bulges. However, the large number of AGN among isolated galaxies is of great importance and indicates that secular evolution processes can trigger/maintain low luminosity AGN activity (see below).

We consider as secular evolution the following mechanisms capable of driving gas into the nuclear region: 1) Minor mergers (luminosity ratio larger than 10 in our sample); 2) Dark matter accretion; 3) Non-axisymmetric gravitational perturbations.

With respect to dark matter, Hernandez & Lee (2010) showed from an analytical treatment of the accretion rate that, for the largest black hole masses of quasi-stellar objects ( $>10^9 M_{\odot}$ ), the runaway regime would be reached on time-scales which are shorter than the lifetimes of the halos in question for central dark matter densities in excess of  $250 M_{\odot}/\text{pc}^3$ . This limit scales inversely with the black hole (BH) mass.

The most common non-axisymmetric internal potential is due to the presence of a bar. However in the particular case of barred galaxies it has been shown that most probably bars do not enhance nuclear activity (Moles et al. 1995; Ho et al. 1997d; Lee et al. 2012). However the samples used in those studies were not rigorously isolated and thus the effects of the environment cannot be disentangled from those of the bar. The samples used in this work provide the opportunity to perform a rigorous test of the effect of a bar. This can be achieved due to both the selection criteria and the quality of the data. A detailed analysis of the bar fraction requires a deep photometric study. This analysis will be presented in a forthcoming paper (Hernández-Toledo et al. in preparation 2013).

We note that although a large fraction of isolated galaxies are active, their SMBH has not grown significantly over the last 3 Gyr. Given that most of

our galaxies are representative of the low luminosity end of AGN, the mass accretion rate should be in the range of  $10^{-5} - 10^{-3} M_{\odot}/\text{yr}$ , and the radiative efficiency  $\eta$  should be significantly smaller than 10 % (Ho 2003, 2009). Such low efficiencies are predicted for low luminosity AGN (Narayan & McClintock 2008). Assuming the AGN in our sample have accreted at a constant rate over the last 3 Gyr the growth of their SMBH ranges between  $10^4 - 10^6 M_{\odot}$ . Then, it is clear that isolated galaxies in poor environments have failed to accrete enough material (at least during the last Gyr) to present higher luminosities and significant black hole growth. Thus, our results support a hierarchical scenario in which the environment is crucial to determine properties such as luminosity, mass, and central SMBH mass, fulfilling the expectations of the downsizing for SMBH growth (Pérez-González et al. 2010).

The spiral isolated galaxies will not migrate from the blue to the red sequence since feedback is not efficient in these faint AGN (Krongold et al. 2007). The later result supports again that secular evolution in these galaxies is the important mechanism to establish the bulge-black hole relation. This is in contrast to the case of massive galaxies transitioning from the blue to the red branch of the color-color diagram which require a major merger followed by a substantial feedback in the QSO phase.

On the other hand our isolated ellipticals are already in the red-branch of galaxies that probably have experienced a major merger in the distant past. The fact that essentially all of them are AGN may simply reflect the fact that it is easier to drive gas to the center of spheroidal systems. The remanent inter stellar medium (ISM) in these galaxies is typically in the range ( $10^6$ - $10^7 M_{\odot}$ ). Therefore, they contain enough gas to power their SMBH over the last 3 Gyr. This does not exclude, however, the possibility of an external supply of material as suggested by several authors (Bertola et al. 1992; Caon et al. 2000; Sarzi et al.

2006). The large fraction of AGN in these galaxies suggests that the presence of a large bulge facilitates the mass in fall to the center. We note, however, that a small fraction of this LINERs could be fake AGN (“retired galaxies”, Cid Fernandes et al. (2011) ).

Finally the absence of type 1 AGN in these samples of isolated galaxies is remarkable and at odds with a simple interpretation of the unified model (UM). There is not a single type 1.0 AGN among the 175 active galaxies in our samples. The fraction of types 1.5-1.9 is less than 3 % in both isolated galaxy samples.

All these results indicate that the presence of AGN activity is a common phenomenon in galaxies independently of the environment. This is an important result as traditionally it has been assumed that an external perturbation is required to induce nuclear activity. Our results indicate that a low luminosity AGN phase is a part of the secular evolution of a large number of galaxies. These findings are consistent with those by Ho et al. (1997a,c); Ho (2002, and references therein). However, in those studies it was impossible to disentangle the environmental effects from those of internal galactic evolution, given that the isolation history was not known a priori in their samples. Our results do not deny the possibility that external perturbations may enhance the frequency of nuclear activity among galaxies, as has been suggested by previous studies (Dultzin-Hacyan et al. 1999; Krongold et al. 2002, 2003; Rogers et al. 2009; Ellison et al. 2010, 2011). The effect of a strong gravitational interaction will be studied in a forthcoming paper where the incidence of AGN in a sample of isolated close pairs of similar mass galaxies will be analyzed. We also note that the lack of high luminosity AGN in our samples points towards a dependence between environment/interactions and AGN luminosity. In this scenario, the extremely low fraction of type 1 AGN can be understood if a BLR (broad line



region) can be formed only at higher accretion rates/luminosities (Nicastro 2000; Elitzur & Ho 2009). The appearance of a type 1 nucleus may be delayed by as much as 1 Gyr, as required by the evolutionary model proposed by Krongold et al. (2007), where an interaction triggers first a circumnuclear starburst, and subsequently non-thermal nuclear activity. For the brightest end of nuclear activity a similar evolutionary trend is possible (from ULIRGs to luminous quasars). In this case a major merger would be required, affecting the overall properties of the host galaxy and moving it to the blue branch of the color-color diagram.

If AGN in isolated galaxies have low accretion rates, low efficiencies, low luminosities and almost a complete absence of broad lines in their spectra, it is probable that the BLR under these circumstances is not even able to form. This is in accordance with the result by Tran (2003a,b) for the absence of broad components in polarized light for  $\sim 50\%$  of the galaxies in his sample. Several studies show evidence that the Sy2s with and without broad lines in polarized lines (in other words with and without a hidden BLR) are truly different in other respects as well (e.g. Gu et al. 2001a,b; Bianchi et al. 2012).

FJHI acknowledges a graduate student scholarship from CONACYT. DD acknowledge support from grant IN111610 PAPIIT, UNAM.

## REFERENCES

- Abazajian, K. N., Adelman-McCarthy, J. K., Agüeros, M. A., et al. 2009, *ApJS*, 182, 543
- Baldwin, J. A., Phillips, M. M., & Terlevich, R. 1981, *PASP*, 93, 5
- Barton, E. J., Geller, M. J., & Kenyon, S. J. 2000, *ApJ*, 530, 660
- Bertola, F., Buson, L. M., & Zeilinger, W. W. 1992, *ApJ*, 401, L79
- Bianchi, S., Panessa, F., Barcons, X., et al. 2012, arXiv:1209.0274
- Binette, L., Drissen, L., Ubeda, L., et al. 2009, *A&A*, 500, 817
- Caon, N., Macchetto, D., & Pastoriza, M. 2000, *ApJS*, 127, 39
- Cid Fernandes, R., Stasińska, G., Mateus, A., & Vale Asari, N. 2011, *MNRAS*, 413, 1687
- Coziol, R., Torres-Papaqui, J. P., Plauchu-Frayn, I., et al. 2011, *Rev. Mexicana Astron. Astrofis.*, 47, 361
- Dahari, O. A. 1984, Ph.D. Thesis,
- Dahari, O. 1985, *ApJS*, 57, 643
- de Mello, D. F., Keel, W. C., Sulentic, J. W., & Rampazzo, R. 1995, *Stellar Populations*, 164, 434
- de Mello, D. F., Sulentic, J. W., de Souza, R. E., Reduzzi, L., & Rampazzo, R. 1996, *A&A*, 308, 387
- Dultzin-Hacyan, D., Krongold, Y., Fuentes-Guridi, I., & Marziani, P. 1999, *ApJ*, 513, L111
- Elitzur, M., & Ho, L. C. 2009, *ApJ*, 701, L91
- Ellison, S. L., Patton, D. R., Simard, L., et al. 2010, *MNRAS*, 407, 1514

- Ellison, S. L., Patton, D. R., Mendel, J. T., & Scudder, J. M. 2011, MNRAS, 418, 2043
- Gu, Q., Dultzin-Hacyan, D., & de Diego, J. A. 2001, Rev. Mexicana Astron. Astrofis., 37, 3
- Gu, Q., Maiolino, R., & Dultzin-Hacyan, D. 2001, A&A, 366, 765
- Hao, L., Strauss, M. A., Tremonti, C. A., et al. 2005, AJ, 129, 1783
- Heckman, T. M. 1980, A&A, 87, 142
- Heckman, T. M. 1980, Highlights of Astronomy, 5, 185
- Hernandez, X., & Lee, W. H. 2010, MNRAS, 404, L6
- Hernández Toledo, H. M., Dultzin-Hacyan, D., Gonzalez, J. J., & Sulentic, J. W. 1999, AJ, 118, 108
- Hernández-Toledo, H. M., Vázquez-Mata, J. A., Martínez-Vázquez, L. A., Choi, Y.-Y., & Park, C. 2010, AJ, 139, 2525
- Ho, L. C., Filippenko, A. V., & Sargent, W. L. W. 1997, ApJS, 112, 315
- Ho, L. C., Filippenko, A. V., Sargent, W. L. W., & Peng, C. Y. 1997, ApJS, 112, 391
- Ho, L. C., Filippenko, A. V., & Sargent, W. L. W. 1997, ApJ, 487, 568
- Ho, L. C., Filippenko, A. V., & Sargent, W. L. W. 1997, ApJ, 487, 591
- Ho, L. C. 2002, IAU Colloq. 184: AGN Surveys, 284, 13
- Ho, L. C. 2003, Active Galactic Nuclei: From Central Engine to Host Galaxy, 290, 379

- Ho, L. C. 2009, *ApJ*, 699, 626
- Karachentsev, I. D., Makarov, D. I., Karachentseva, V. E., & Melnyk, O. V. 2011, *Astrophysical Bulletin*, 66, 1
- Karachentseva, V. E. 1973, *Soobshcheniya Spetsial'noj Astrofizicheskoy Observatorii*, 8, 3
- Karachentseva, V. E., Mitronova, S. N., Melnyk, O. V., & Karachentsev, I. D. 2010, *Galaxies in Isolation: Exploring Nature Versus Nurture*, 421, 11
- Kauffmann, G. 2003, *MNRAS*, 346, 1055
- Keel, W. C. 1983, *ApJ*, 269, 466
- Keel, W. C. 1993, *AJ*, 106, 1771
- Kennicutt, R. C., Jr., & Keel, W. C. 1984, *ApJ*, 279, L5
- Kennicutt, R. C., Jr., Roettiger, K. A., Keel, W. C., van der Hulst, J. M., & Hummel, E. 1987, *AJ*, 93, 1011
- Kewley, L. J., Dopita, M. A., Sutherland, R. S., Heisler, C. A., & Trevena, J. 2001, *ApJ*, 556, 121
- Koulouridis, E., Chavushyan, V., Plionis, M., Krongold, Y., & Dultzin-Hacyan, D. 2006, *ApJ*, 651, 93
- Koulouridis, E., Plionis, M., Chavushyan, V., et al. 2006, *ApJ*, 639, 37
- Krongold, Y., Dultzin-Hacyan, D., & Marziani, P. 2001, *AJ*, 121, 702
- Krongold, Y., Dultzin-Hacyan, D., & Marziani, P. 2002, *ApJ*, 572, 169
- Krongold, Y., Dultzin-Hacyan, D., & Marziani, P. 2003, *Active Galactic Nuclei: From Central Engine to Host Galaxy*, 290, 523

- Krongold, Y., Nicastro, F., Elvis, M., et al. 2007, *ApJ*, 659, 1022
- Laurikainen, E., & Salo, H. 1995, *A&A*, 293, 683
- Lee, G.-H., Woo, J.-H., Lee, M. G., et al. 2012, arXiv:1203.1693
- Lin, L., Koo, D. C., Weiner, B. J., et al. 2007, *ApJ*, 660, L51
- Lonsdale, C. J., Persson, S. E., & Matthews, K. 1984, *ApJ*, 287, 95
- Márquez, I., & Masegosa, J. 2008, *Revista Mexicana de Astronomía y Astrofísica Conference Series*, 32, 150
- Martínez, M. A., Del Olmo, A., Coziol, R., & Perea, J. 2010, *AJ*, 139, 1199
- Miller, C. J., Nichol, R. C., Gómez, P. L., Hopkins, A. M., & Bernardi, M. 2003, *ApJ*, 597, 142
- Moles, M., Marquez, I., & Perez, E. 1995, *ApJ*, 438, 604
- Narayan, R., & McClintock, J. E. 2008, *New A Rev.*, 51, 733
- Nicastro, F. 2000, *ApJ*, 530, L65
- Pérez-González, P. G., Alonso-Herrero, A., Donley, J., et al. 2010, *Highlights of Spanish Astrophysics V*, 337
- Rogers, B., Ferreras, I., Kaviraj, S., Pasquali, A., & Sarzi, M. 2009, *MNRAS*, 399, 2172
- Sabater, J., Verdes-Montenegro, L., Leon, S., Best, P., & Sulentic, J. 2012, *A&A*, 545, A15
- Sarzi, M., Falcón-Barroso, J., Davies, R. L., et al. 2006, *MNRAS*, 366, 1151
- Schmitt, H. R. 2001, *AJ*, 122, 2243
- Shapovalova, A. I., Popović, L. Č., Collin, S., et al. 2008, *A&A*, 486, 99

- Shapovalova, A. I., Popović, L. Č., Burenkov, A. N., et al. 2012, *ApJS*, 202, 10
- Sorrentino, G., Radovich, M., & Rifatto, A. 2006, *A&A*, 451, 809
- Stasińska, G., Cid Fernandes, R., Mateus, A., Sodré, L., & Asari, N. V. 2006, *MNRAS*, 371, 972
- Stauffer, J. R. 1982, *ApJS*, 50, 517
- Stauffer, J. R. 1982, *ApJ*, 262, 66
- Storchi-Bergmann, T. 2008, *Revista Mexicana de Astronomia y Astrofisica Conference Series*, 32, 139
- Sulentic, J. W., Verdes-Montenegro, L., Bergond, G., et al. 2006, *A&A*, 449, 937
- Tran, H. D. 2003, *ApJ*, 583, 632
- Tran, H. D. 2003, *Active Galactic Nuclei: From Central Engine to Host Galaxy*, 290, 31
- Trouille, L., Barger, A. J., & Tremonti, C. 2011, *ApJ*, 742, 46
- Varela, J., Moles, M., Márquez, I., et al. 2004, *A&A*, 420, 873
- Veilleux, S., & Osterbrock, D. E. 1987, *ApJS*, 63, 295
- Verdes-Montenegro, L., Sulentic, J., Lisenfeld, U., et al. 2005, *A&A*, 436, 443
- Verley, S., Leon, S., Verdes-Montenegro, L., et al. 2007, *A&A*, 472, 121
- Winkler, H. 1992, *MNRAS*, 257, 677
- Woods, D. F., & Geller, M. J. 2007, *AJ*, 134, 527

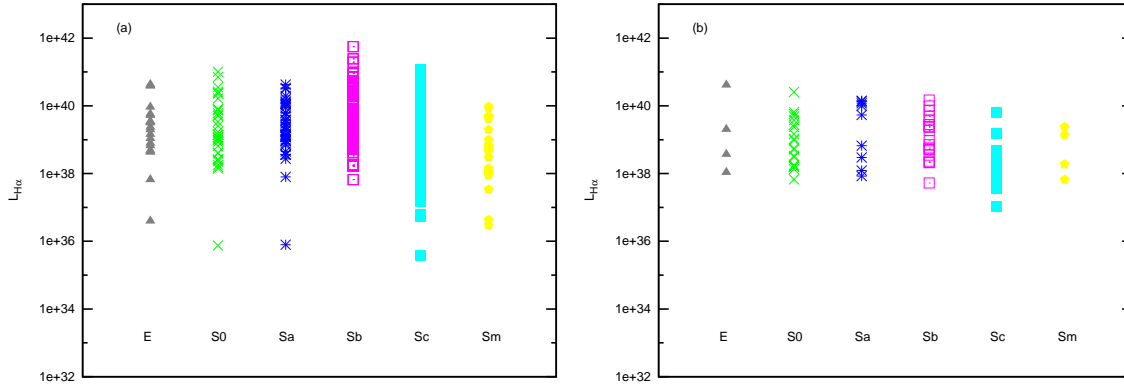


Fig. 1.— Morphological distribution of H $\alpha$  luminosity for (a) CIG sample and (b) Varela's sample. Mean values of AGN H $\alpha$  luminosity for CIG and Varela's samples are  $L_{H\alpha} = 9.2 \times 10^{39}$  erg s $^{-1}$  and  $L_{H\alpha} = 1.8 \times 10^{39}$  erg s $^{-1}$  respectively which correspond to Low Luminosity AGN.

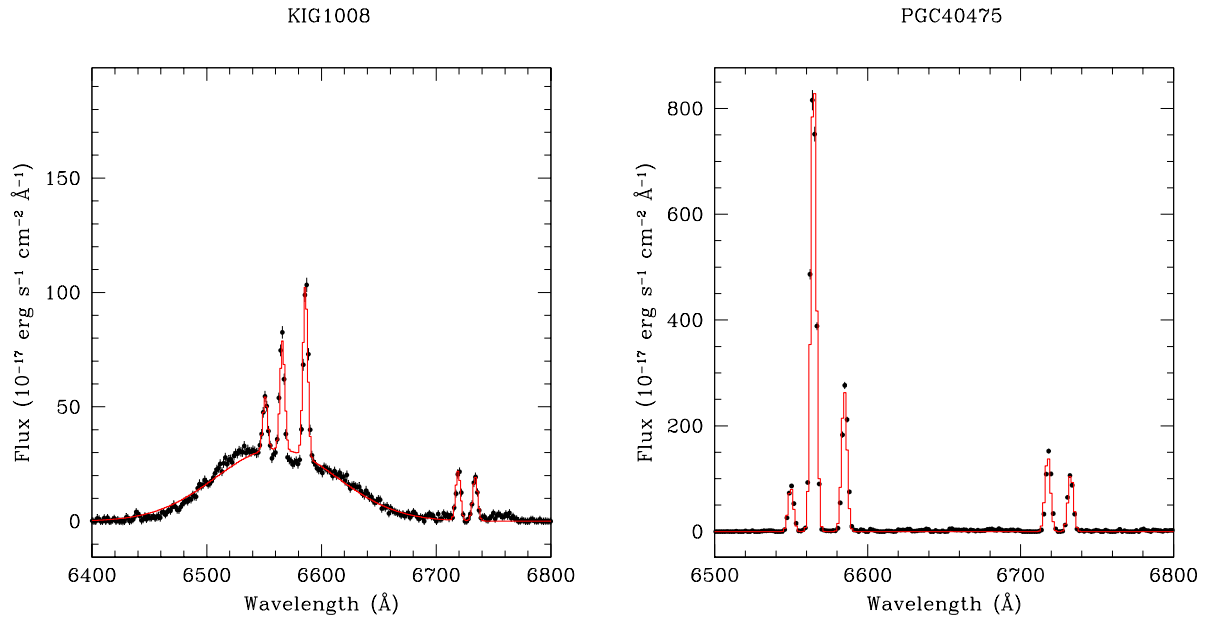


Fig. 2.— Examples of fits in H $\alpha$  region for galaxies with and without broad line respectively. Black data points denote the spectrum with the stellar contribution subtracted and the red line shows the fit.



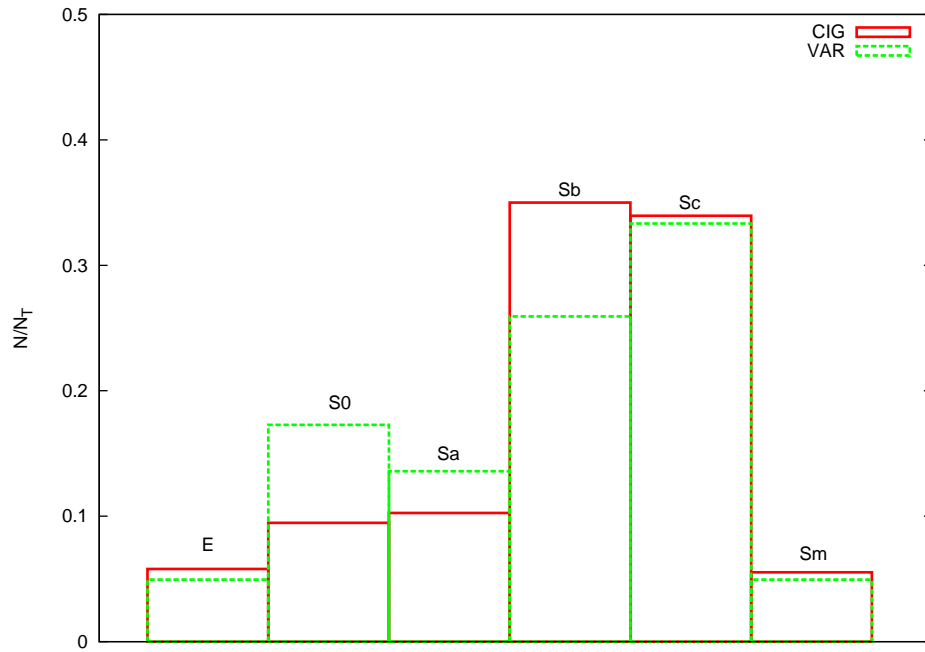


Fig. 3.— Histogram of our samples with morphological type separation. Continuous red line correspond to CIG sample and dashed green line to Varela's sample.

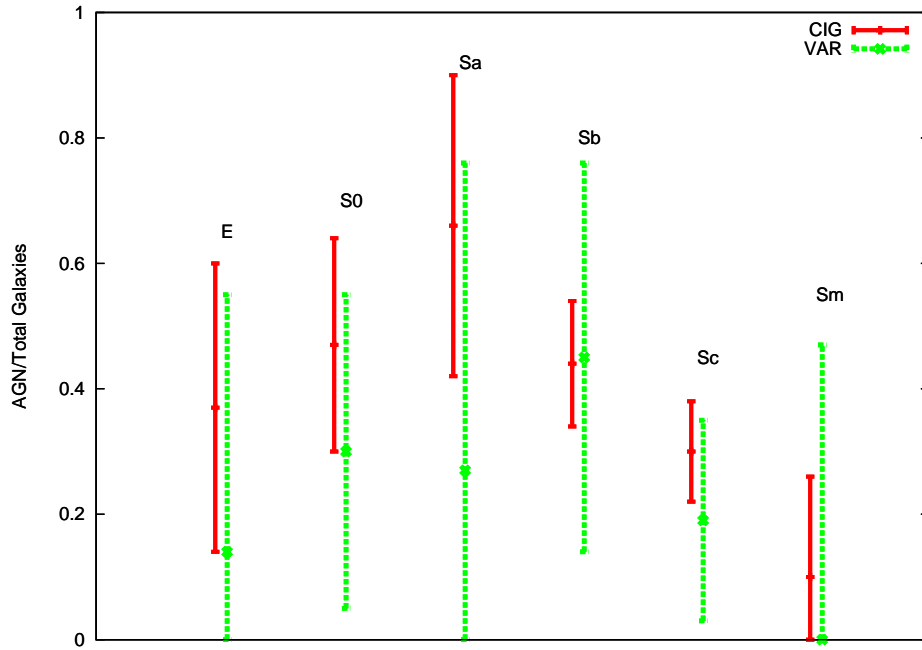


Fig. 4.— Statistical comparison between isolated samples. Lines labels like in Figure 3.

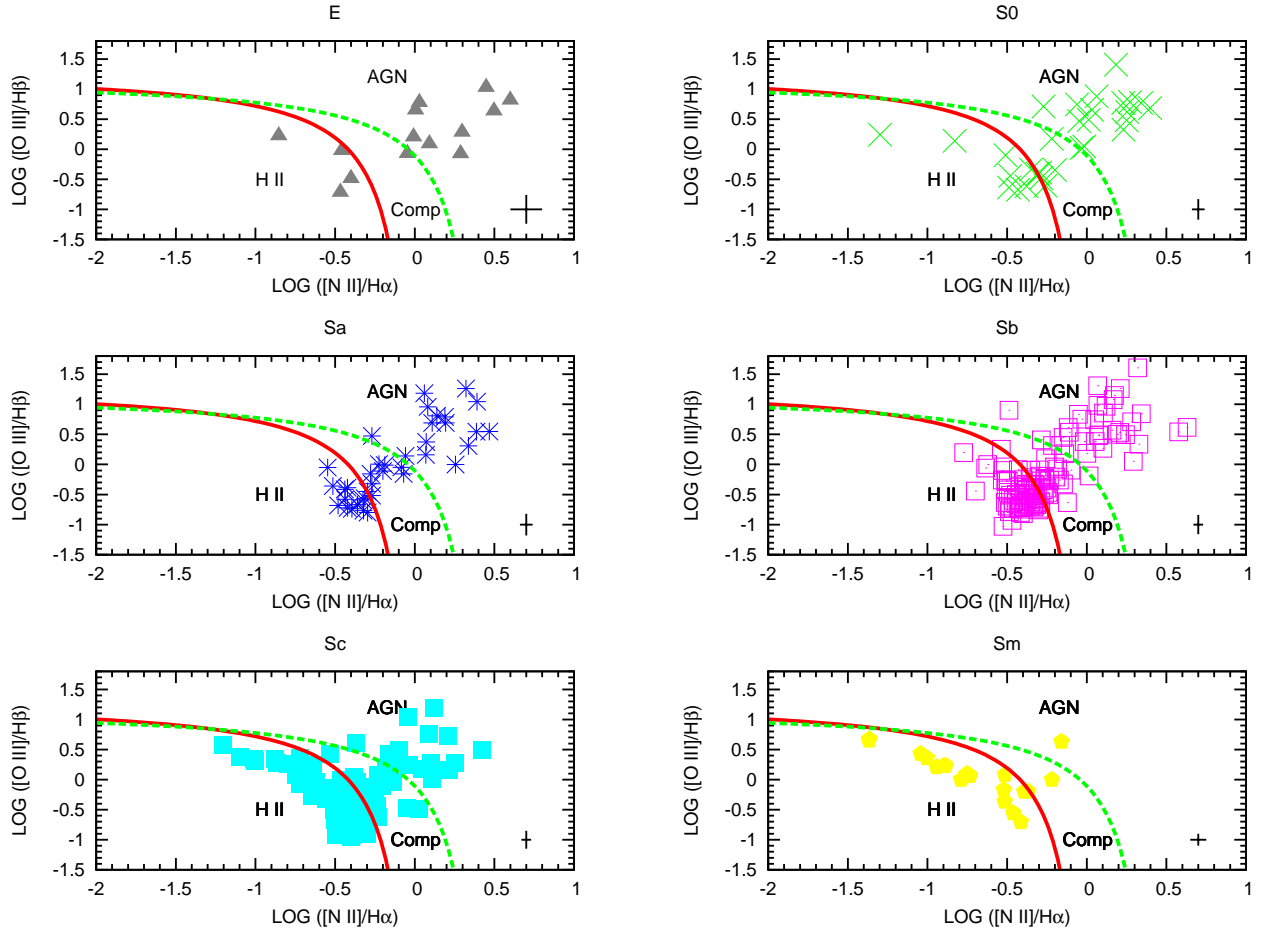


Fig. 5.— The  $[\text{N II}]$  diagnostic diagrams for CIG sample with different morphologies. This diagram separates between three different kind of activity in galaxies like AGN, Composite and H II like region galaxies. The green dashed line (Ke01) separates galaxies with a AGN from Composite (AGN+Starburts activity). Continuous red line (Ka03) divides pure star forming galaxies from AGN-starburts composite objects. Elliptical galaxies are shown as filled gray triangles, lenticular as green crosses, Sa as blue asterisks, Sb as pink empty squares, Sc as filled cyan squares and Sm as filled yellow pentagons. The cross at the lower right part of the diagram is the mean error in the line ratios.

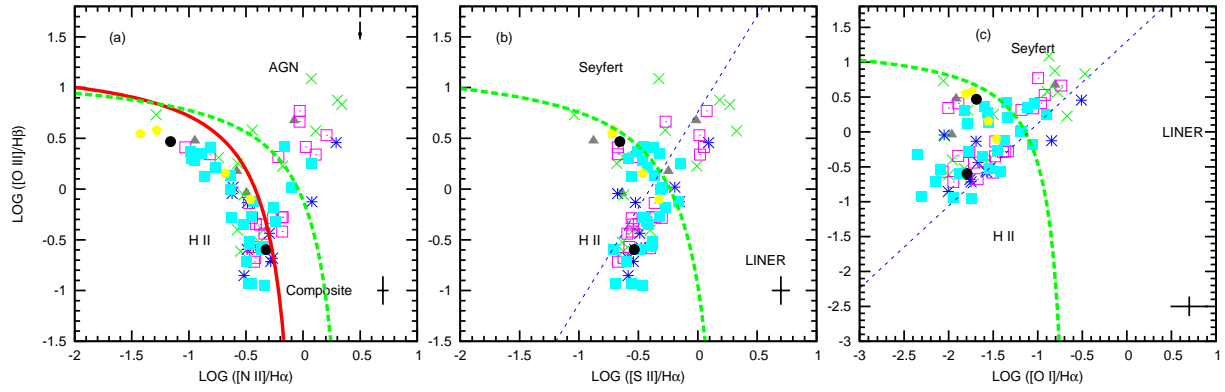


Fig. 6.— (a) The [N II], (b) [S II] and (c) [O I] diagnostic diagrams for Varela’s sample. Labels like on Figure 5. The low incidence of nuclear activity are present on Sc and Sm types. Filled circles represent objects which cannot be classified.

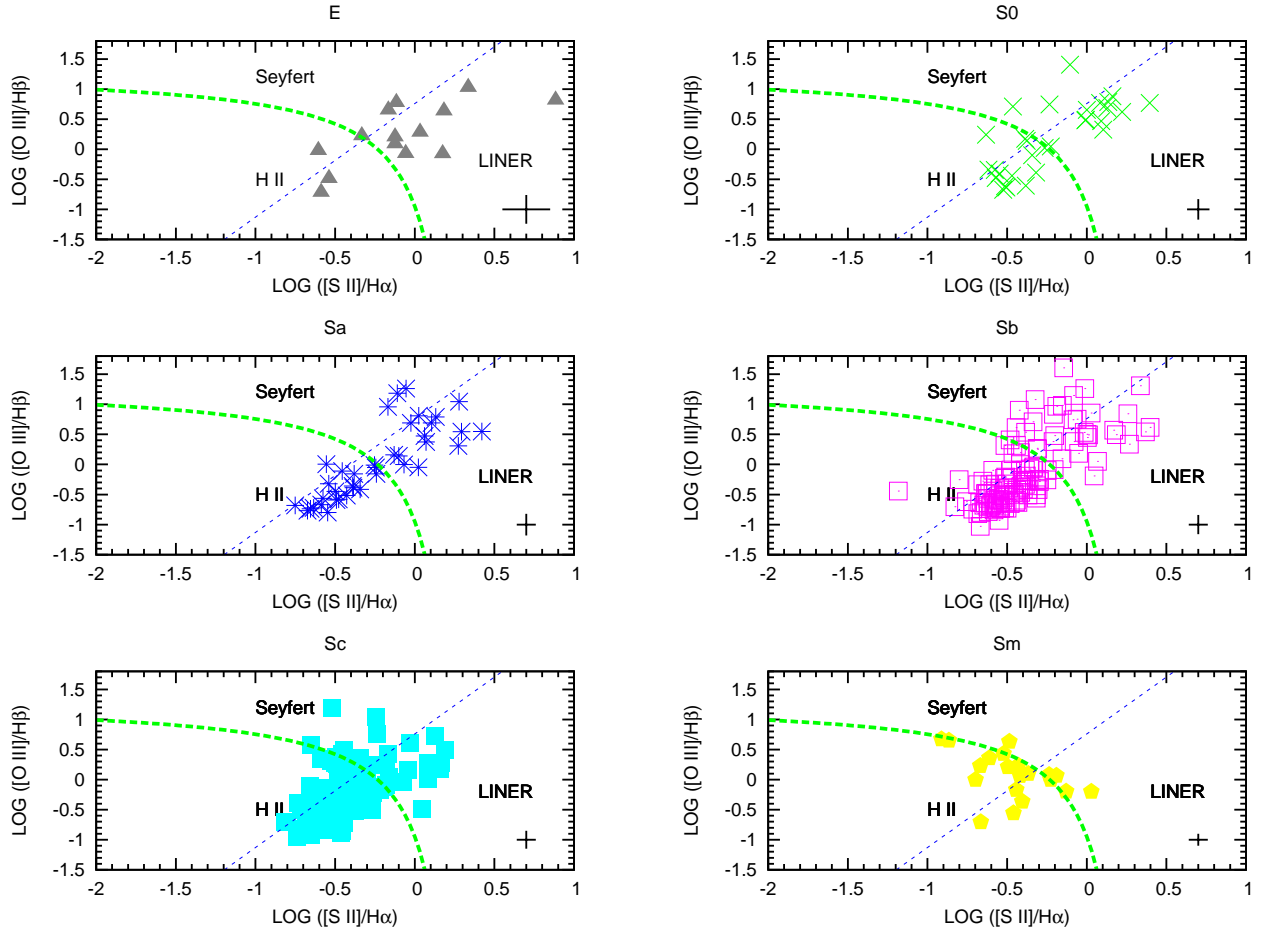


Fig. 7.— The [S II] diagnostic diagram for CIG sample. Blue dashed line represents Seyfert/LINER line and others labels like in Figure 5.

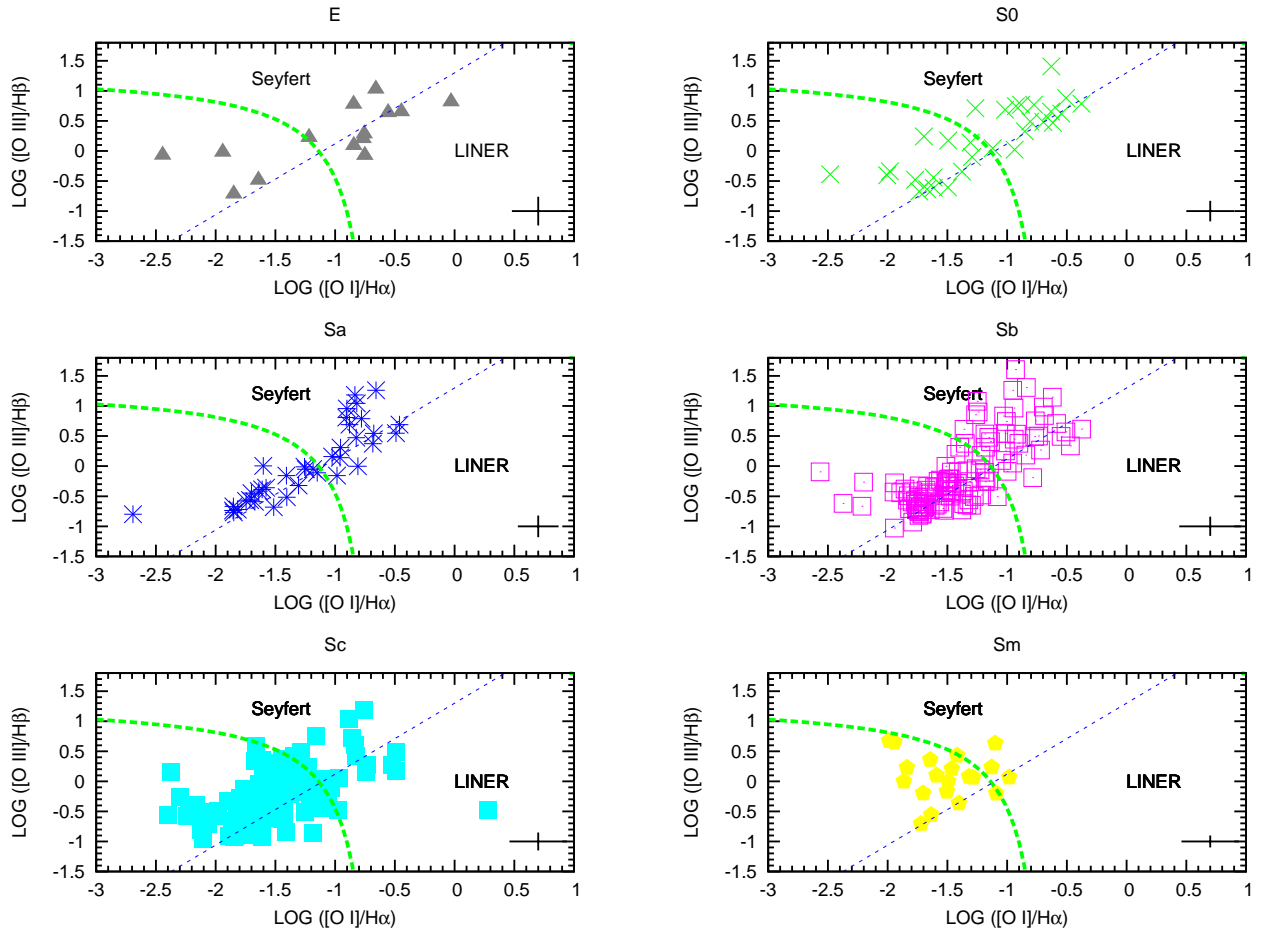


Fig. 8.— The [O I] diagnostic diagram for CIG sample. Labels like on Figure 7.

Table 1. General statistics of both Isolated galaxy samples.

Sample	Total	No Emission	Excluded	Fitted	AGN+Comp	H II	AGN Type 1
CIG	413	18(4%)	47(11%)	348(84%)	150(36%)	198(48%)	12(3%)
VAR	100	10(10%)	7(7%)	83(83%)	26(26%)	57(57%)	1(1%)
TOTAL	513	28(5%)	54(11%)	431(84%)	176(34%)	255(50%)	13(3%)

Table 2: Morphology distribution and incidence of nuclear activity for the CIG sample derived from [N II] BPT diagnostic diagram.

M.T.	Galaxies with Emission lines				Total sample			
	Total	H II	Comp	AGN+Comp	Total	H II	Comp	AGN+Comp
E	14	4(29%)	1(7%)	10(71%)	23	4(17%)	1(4%)	10(43%)
S0	30	9(30%)	5(17%)	21(70%)	38	9(24%)	5(13%)	21(55%)
Sa	38	13(34%)	8(21%)	25(66%)	38	13(34%)	8(21%)	25(66%)
Sb	122	67(55%)	20(16%)	55(45%)	124	67(54%)	20(16%)	55(44%)
Sc	124	87(70%)	22(18%)	37(30%)	124	87(70%)	22(18%)	37(30%)
Sm	20	18(90%)	1(5%)	2(10%)	20	18(90%)	1(5%)	2(10%)
Total	348	198(57%)	57(16%)	150(43%)	367	198(54%)	57(16%)	150(41%)

Table 3: Morphology distribution and incidence of nuclear activity in Varela’s sample derived from [N II] BPT diagnostic diagram.

M.T.	Galaxies with Emission lines				Total sample			
	Total	H II	Comp	AGN+Comp	Total	H II	Comp	AGN+Comp
E	4	3(75%)	0(0%)	1(25%)	7	3(43%)	0(0%)	1(14%)
S0	14	8(57%)	1(7%)	6(43%)	20	8(40%)	1(5%)	6(30%)
Sa	11	8(73%)	1(9%)	3(27%)	11	8(73%)	1(9%)	3(27%)
Sb	21	11(52%)	4(19%)	10(48%)	22	11(50%)	4(18%)	10(45%)
Sc	27	22(81%)	3(11%)	5(19%)	27	22(81%)	3(11%)	5(19%)
Sm	4	4(100%)	0(0%)	0(0%)	4	4(100%)	0(0%)	0(0%)
Total	81	56(69%)	9(11%)	25(31%)	91	56(62%)	9(10%)	25(27%)



Table 4: Incidence type of nuclear activity for different morphologies from [S II] and [O I] diagnostic diagrams for CIG sample.

M.T.	[S II] Diagram				[O I] Diagram			
	Total	AGN	Seyfert	LINER	Total	AGN	Seyfert	LINER
E	14	11(79%)	3(27%)	8(73%)	13	10(77%)	3(30%)	7(70%)
S0	30	15(50%)	3(20%)	12(80%)	28	16(57%)	12(75%)	4(25%)
Sa	38	15(39%)	3(20%)	12(80%)	36	17(47%)	11(65%)	6(35%)
Sb	122	31(27%)	15(48%)	16(52%)	120	39(33%)	30(77%)	9(23%)
Sc	124	21(17%)	8(38%)	13(62%)	123	22(18%)	11(50%)	11(50%)
Sm	20	6(30%)	1(17%)	5(83%)	20	3(15%)	2(67%)	1(33%)
Total	348	99(28%)	33(33%)	66(67%)	340	107(31%)	69(64%)	38(36%)

Table 5: Incidence type of nuclear activity for different morphologies from [S II] and [O I] diagnostic diagrams for Varela’s sample.

M.T.	[S II] Diagram				[O I] Diagram			
	Total	AGN	Seyfert	LINER	Total	AGN	Seyfert	LINER
E	4	2(50%)	0(0%)	2(100%)	4	1(25%)	1(100%)	0(0%)
S0	14	6(43%)	2(33%)	4(67%)	14	6(43%)	5(83%)	1(17%)
Sa	11	3(27%)	0(0%)	3(100%)	11	2(18%)	0(0%)	2(100%)
Sb	21	5(24%)	1(20%)	4(80%)	21	6(29%)	6(100%)	0(0%)
Sc	27	5(19%)	3(60%)	2(40%)	27	5(19%)	4(80%)	1(20%)
Sm	4	0(0%)	0(0%)	0(0%)	4	0(0%)	0(0%)	0(0%)
Total	81	21(26%)	6(29%)	15(71%)	81	20(25%)	16(80%)	4(20%)

Table 6. Logarithm intensity ratios with their errors and AGN type for the CIG sample.

Object	M.T. <sup>a</sup>	LOG([O III]/H $\beta$ )	LOG([N II]/H $\alpha$ )	LOG([S II]/H $\alpha$ )	LOG([O I]/H $\alpha$ )	Type
Elliptical						
KIG378	E	0.2831 $\pm$ 0.1763	0.2970 $\pm$ 0.0806	0.0332 $\pm$ 0.1534	-0.7559 $\pm$ 0.3383	LINER
KIG393	E-SO	-0.0234 $\pm$ 0.0074	-0.4586 $\pm$ 0.0066	-0.6059 $\pm$ 0.0091	-1.9412 $\pm$ 0.0287	HII
KIG437	E-SO	0.0909 $\pm$ 0.1939	0.0919 $\pm$ 0.0589	-0.1233 $\pm$ 0.1182	-0.8432 $\pm$ 0.2380	LINER
KIG462	E	-0.7172 $\pm$ 0.0384	-0.4667 $\pm$ 0.0098	-0.5874 $\pm$ 0.0155	-1.8481 $\pm$ 0.0740	HII
KIG555	E	0.2234 $\pm$ 0.0401	-0.8536 $\pm$ 0.0429	-0.3324 $\pm$ 0.0298	-1.2193 $\pm$ 0.0865	HII
KIG556	E	0.8151 $\pm$ 0.5101	0.5997 $\pm$ 0.2621	0.8841 $\pm$ 0.2651	-0.0295 $\pm$ 0.4288	LINER
KIG582	E	1.0277 $\pm$ 0.6437	0.4476 $\pm$ 0.1483	0.3357 $\pm$ 0.2130	-0.6587 $\pm$ 0.5464	LINER
KIG595	E	-0.0732 $\pm$ 0.2877	-0.0465 $\pm$ 0.2346	-0.0569 $\pm$ 0.3745	-	LINER
KIG602	E	0.2051 $\pm$ 0.1068	-0.0084 $\pm$ 0.0247	-0.1233 $\pm$ 0.0420	-0.7662 $\pm$ 0.0711	LINER
KIG685	E	-0.0750 $\pm$ 0.1945	0.2877 $\pm$ 0.2436	0.1754 $\pm$ 0.3742	-0.7523 $\pm$ 1.0180	LINER
KIG705	E	0.6353 $\pm$ 0.5484	0.4970 $\pm$ 0.0898	0.1829 $\pm$ 0.1587	-0.5566 $\pm$ 0.3031	LINER
KIG735	E-SO	0.6529 $\pm$ 0.3846	0.0049 $\pm$ 0.1637	-0.1656 $\pm$ 0.3282	-0.4449 $\pm$ 0.3062	L-S $\dagger$
KIG768	E	-0.4878 $\pm$ 0.0242	-0.4003 $\pm$ 0.0090	-0.5381 $\pm$ 0.0142	-1.6419 $\pm$ 0.0481	HII
KIG1029	E	0.7769 $\pm$ 0.2027	0.0280 $\pm$ 0.0334	-0.1154 $\pm$ 0.0598	-0.8457 $\pm$ 0.1231	Sy2
Spheroidal						
KIG213	S0a	0.4819 $\pm$ 0.1403	0.2505 $\pm$ 0.0532	-0.0091 $\pm$ 0.1031	-0.6965 $\pm$ 0.1868	S-L $\dagger$
KIG228	S0	-0.3462 $\pm$ 0.1376	-0.2004 $\pm$ 0.0294	-0.5771 $\pm$ 0.0894	-1.3772 $\pm$ 0.2291	AGN
KIG244	S0-a	-0.4046 $\pm$ 0.1778	-0.3080 $\pm$ 0.0441	-0.5467 $\pm$ 0.1134	-2.0040 $\pm$ 1.2503	HII
KIG272	S0-a	-0.6374 $\pm$ 0.0387	-0.4888 $\pm$ 0.0104	-0.5050 $\pm$ 0.0158	-1.6710 $\pm$ 0.0644	HII
KIG332	S0	0.7437 $\pm$ 0.0367	-0.0622 $\pm$ 0.0176	-0.2335 $\pm$ 0.0310	-0.9269 $\pm$ 0.0562	Sy2
KIG338	S0	0.6551 $\pm$ 0.2278	0.0325 $\pm$ 0.0833	0.0000 $\pm$ 0.1304	-0.6331 $\pm$ 0.2261	S-L $\dagger$
KIG349	S0-a	0.3299 $\pm$ 0.0320	-0.1181 $\pm$ 0.0072	-0.2973 $\pm$ 0.0126	-1.1286 $\pm$ 0.0261	Sy1.9
KIG394	S0-a	0.1737 $\pm$ 0.0405	-0.2196 $\pm$ 0.0171	-0.3860 $\pm$ 0.0321	-1.4940 $\pm$ 0.1219	AGN
KIG413	S0-a	0.7853 $\pm$ 0.5114	0.2708 $\pm$ 0.0746	0.1349 $\pm$ 0.1219	-0.3785 $\pm$ 0.1575	S-L $\dagger$

Table 6—Continued

Object	M.T. <sup>a</sup>	LOG([O III]/H $\beta$ )	LOG([N II]/H $\alpha$ )	LOG([S II]/H $\alpha$ )	LOG([O I]/H $\alpha$ )	Type
KIG441	S0-a	-0.1001 $\pm$ 0.0430	-0.5103 $\pm$ 0.0184	-0.3426 $\pm$ 0.0245	-1.2934 $\pm$ 0.0697	HII
KIG460	S0-a	-0.4401 $\pm$ 0.0373	-0.4800 $\pm$ 0.0120	-0.4691 $\pm$ 0.0181	-1.6159 $\pm$ 0.0721	HII
KIG480	S0-a	0.4907 $\pm$ 0.0396	0.0117 $\pm$ 0.0140	-0.0060 $\pm$ 0.0200	-0.8059 $\pm$ 0.0399	S-L $\dagger$
KIG483	S0	0.3258 $\pm$ 0.2015	0.2305 $\pm$ 0.0747	0.1035 $\pm$ 0.1225	-0.8513 $\pm$ 0.3551	LINER
KIG485	S0	0.7681 $\pm$ 0.1890	0.3413 $\pm$ 0.1876	0.3951 $\pm$ 0.2365	-0.8834 $\pm$ 1.0911	S-L $\dagger$
KIG501	S0-a	0.0201 $\pm$ 0.1278	-0.0320 $\pm$ 0.0430	-0.2650 $\pm$ 0.0960	-0.9375 $\pm$ 0.1773	LINER
KIG504	S0-a	-0.6740 $\pm$ 0.0316	-0.4325 $\pm$ 0.0086	-0.5243 $\pm$ 0.0135	-1.7358 $\pm$ 0.0537	HII
KIG571	S0	-0.6063 $\pm$ 0.3602	-0.2589 $\pm$ 0.0405	-0.3824 $\pm$ 0.0783	-1.4961 $\pm$ 0.4203	AGN
KIG577	S0	0.2411 $\pm$ 0.0122	-1.2983 $\pm$ 0.0253	-0.6328 $\pm$ 0.0151	-1.6963 $\pm$ 0.0596	HII
KIG586	S0	0.7678 $\pm$ 1.1443	0.2291 $\pm$ 0.0869	0.0838 $\pm$ 0.1498	-0.7745 $\pm$ 0.3665	S-L $\dagger$
KIG591	S0-a	0.7111 $\pm$ 0.0342	-0.2711 $\pm$ 0.0097	-0.4634 $\pm$ 0.0129	-1.2657 $\pm$ 0.0211	S-L $\dagger$
KIG592	S0	-0.4802 $\pm$ 0.0135	-0.2864 $\pm$ 0.0049	-0.5709 $\pm$ 0.0084	-1.7710 $\pm$ 0.0342	AGN
KIG614	S0	0.6198 $\pm$ 0.3960	0.2532 $\pm$ 0.0730	0.2217 $\pm$ 0.1040	-0.5475 $\pm$ 0.1990	LINER
KIG616	S0-a	0.0445 $\pm$ 0.1190	-0.0163 $\pm$ 0.0317	-0.2263 $\pm$ 0.0646	-1.1197 $\pm$ 0.1822	AGN
KIG665	S0-a	-0.3872 $\pm$ 0.2416	-0.2928 $\pm$ 0.0334	-0.3188 $\pm$ 0.0597	-	AGN
KIG678	S0-a	-0.3386 $\pm$ 0.0098	-0.3503 $\pm$ 0.0050	-0.6172 $\pm$ 0.0078	-1.9816 $\pm$ 0.0325	HII
KIG697	S0	0.6852 $\pm$ 0.1816	0.3973 $\pm$ 0.1063	0.1287 $\pm$ 0.1877	-1.0169 $\pm$ 0.8012	S-L $\dagger$
KIG698	S0-a	0.8826 $\pm$ 0.3627	0.0618 $\pm$ 0.1145	0.1613 $\pm$ 0.1473	-0.5063 $\pm$ 0.2470	S-L $\dagger$
KIG893	S0	1.4052 $\pm$ 0.0713	0.1830 $\pm$ 0.0197	-0.1051 $\pm$ 0.0382	-0.6296 $\pm$ 0.0517	Sy2
KIG903	S0	0.4668 $\pm$ 0.0943	-0.0474 $\pm$ 0.0432	0.0909 $\pm$ 0.0539	-0.6165 $\pm$ 0.0963	LINER
KIG1014	S0-a	-0.6140 $\pm$ 0.0522	-0.3787 $\pm$ 0.0114	-0.5127 $\pm$ 0.0204	-1.6142 $\pm$ 0.0813	HII
KIG1032	S0-a	0.1383 $\pm$ 0.0203	-0.8297 $\pm$ 0.0181	-0.3772 $\pm$ 0.0150	-1.3063 $\pm$ 0.0422	HII
Sa						
KIG60	Sab	-0.3866 $\pm$ 0.0555	-0.4230 $\pm$ 0.0172	-0.3848 $\pm$ 0.0253	-1.6110 $\pm$ 0.1263	HII
KIG223	Sa	-0.6819 $\pm$ 0.1626	-0.4807 $\pm$ 0.0272	-0.7504 $\pm$ 0.0713	-1.5133 $\pm$ 0.1730	HII

Table 6—Continued

Object	M.T. <sup>a</sup>	LOG([O III]/H $\beta$ )	LOG([N II]/H $\alpha$ )	LOG([S II]/H $\alpha$ )	LOG([O I]/H $\alpha$ )	Type
KIG231	Sab	$-0.5167 \pm 0.0964$	$-0.2686 \pm 0.0164$	$-0.4271 \pm 0.0323$	$-1.4044 \pm 0.0995$	AGN
KIG236	SBa	$-0.7215 \pm 0.0548$	$-0.4210 \pm 0.0119$	$-0.6344 \pm 0.0232$	$-1.8161 \pm 0.1170$	HII
KIG258	SBab	$-0.5920 \pm 0.0248$	$-0.3249 \pm 0.0085$	$-0.4913 \pm 0.0129$	$-1.6713 \pm 0.0451$	HII
KIG285	SBab	$1.0432 \pm 0.4782$	$0.3912 \pm 0.0760$	$0.2782 \pm 0.1113$	$-0.8187 \pm 0.3631$	S-L†
KIG287	SABa	$-0.6678 \pm 0.0682$	$-0.3596 \pm 0.0102$	$-0.5863 \pm 0.0211$	$-1.8515 \pm 0.1293$	HII
KIG298	SBa	$-0.0011 \pm 0.1879$	$0.2557 \pm 0.0732$	$-0.0676 \pm 0.1584$	$-0.8098 \pm 0.3546$	LINER
KIG304	SBab	$-0.1576 \pm 0.1155$	$-0.2774 \pm 0.0276$	$-0.3806 \pm 0.0509$	$-1.4082 \pm 0.2109$	AGN
KIG327	Sab	$1.1816 \pm 1.2340$	$0.0599 \pm 0.0641$	$-0.1092 \pm 0.1248$	$-0.8344 \pm 0.2536$	Sy2
KIG334	Sab	$0.4732 \pm 0.2825$	$-0.2691 \pm 0.0651$	$0.0610 \pm 0.0682$	$-0.8230 \pm 0.1900$	S-L†
KIG351	Sab	$0.1406 \pm 0.2719$	$-0.0577 \pm 0.0659$	$-0.1010 \pm 0.1179$	$-0.9593 \pm 0.3057$	LINER
KIG374	Sab	$-0.1091 \pm 0.0600$	$-0.2005 \pm 0.0174$	$-0.4553 \pm 0.0437$	$-1.1498 \pm 0.0908$	AGN
KIG456	Sa	$0.1581 \pm 0.1621$	$0.0700 \pm 0.0371$	$-0.1297 \pm 0.0720$	$-1.0251 \pm 0.2010$	LINER
KIG475	Sab	$0.6911 \pm 0.5663$	$0.1942 \pm 0.0818$	$-0.0247 \pm 0.1525$	$-0.4609 \pm 0.1821$	S-L†
KIG491	SABa	$-0.5626 \pm 0.0523$	$-0.3131 \pm 0.0105$	$-0.5756 \pm 0.0218$	$-1.7119 \pm 0.0938$	HII
KIG500	Sab	$0.5456 \pm 0.2248$	$0.4682 \pm 0.0888$	$0.4216 \pm 0.1182$	$-0.4914 \pm 0.2584$	LINER
KIG505	Sab	$-0.3583 \pm 0.0419$	$-0.5140 \pm 0.0156$	$-0.3898 \pm 0.0199$	$-1.5789 \pm 0.0897$	HII
KIG539	Sab	$0.8060 \pm 0.3284$	$0.1381 \pm 0.0699$	$0.0253 \pm 0.1168$	$-0.9064 \pm 0.3378$	Sy2
KIG544	SBa	$0.9565 \pm 0.0199$	$0.0818 \pm 0.0132$	$-0.1683 \pm 0.0233$	$-0.9021 \pm 0.0433$	Sy2
KIG579	Sab	$0.6906 \pm 0.1883$	$0.1090 \pm 0.0857$	$0.1058 \pm 0.1273$	$-0.8792 \pm 0.3909$	S-L†
KIG587	Sab	$-0.0494 \pm 0.1044$	$-0.0844 \pm 0.0513$	$0.0225 \pm 0.0683$	$-1.1843 \pm 0.3363$	LINER
KIG596	Sab	$0.5441 \pm 0.2149$	$0.3872 \pm 0.0477$	$0.2939 \pm 0.0681$	$-0.6766 \pm 0.1792$	LINER
KIG605	SBab	$0.3735 \pm 0.0829$	$0.0719 \pm 0.0317$	$0.0704 \pm 0.0445$	$-0.6850 \pm 0.0857$	LINER*
KIG609	Sab	$-0.4148 \pm 0.0592$	$-0.4391 \pm 0.0184$	$-0.3427 \pm 0.0241$	$-1.6384 \pm 0.1414$	HII
KIG620	Sa	$-0.7380 \pm 0.0371$	$-0.3948 \pm 0.0095$	$-0.6545 \pm 0.0177$	$-1.8541 \pm 0.0793$	HII
KIG622	SBa	$-0.4486 \pm 0.0280$	$-0.2958 \pm 0.0094$	$-0.4994 \pm 0.0158$	$-1.7003 \pm 0.0676$	AGN

Table 6—Continued

Object	M.T. <sup>a</sup>	LOG([O III]/H $\beta$ )	LOG([N II]/H $\alpha$ )	LOG([S II]/H $\alpha$ )	LOG([O I]/H $\alpha$ )	Type
KIG633	Sa	-0.5798 $\pm$ 0.0375	-0.4364 $\pm$ 0.0117	-0.4775 $\pm$ 0.0179	-1.7460 $\pm$ 0.0978	HII
KIG641	SBa	-0.1560 $\pm$ 0.0356	-0.0700 $\pm$ 0.0117	-0.2408 $\pm$ 0.0209	-0.9847 $\pm$ 0.0409	LINER
KIG643	Sab	1.2605 $\pm$ 0.1875	0.3219 $\pm$ 0.0394	-0.0545 $\pm$ 0.0832	-0.6583 $\pm$ 0.1328	AGN
KIG669	Sa	-0.0118 $\pm$ 0.0445	-0.1884 $\pm$ 0.0128	-0.2522 $\pm$ 0.0163	-1.2563 $\pm$ 0.0363	AGN
KIG689	Sa	-0.0512 $\pm$ 0.0503	-0.5467 $\pm$ 0.0273	-0.2447 $\pm$ 0.0290	-1.2447 $\pm$ 0.0911	HII
KIG690	Sa	-0.3202 $\pm$ 0.2628	-0.2693 $\pm$ 0.0435	-0.5399 $\pm$ 0.1168	-1.3068 $\pm$ 0.2894	AGN
KIG694	Sa	0.3090 $\pm$ 0.1477	0.3362 $\pm$ 0.0473	0.2738 $\pm$ 0.0670	-0.9554 $\pm$ 0.2908	S-L $\dagger$
KIG695	Sa	-0.8004 $\pm$ 0.2952	-0.2958 $\pm$ 0.0331	-0.5470 $\pm$ 0.0828	-	HII
KIG696	Sab	0.7896 $\pm$ 0.5096	0.1894 $\pm$ 0.0604	0.1316 $\pm$ 0.0927	-0.7796 $\pm$ 0.2419	S-L $\dagger$
KIG726	SBa	0.0040 $\pm$ 0.0216	-0.2250 $\pm$ 0.0085	-0.5556 $\pm$ 0.0171	-1.6008 $\pm$ 0.0601	LINER
KIG751	Sa	-0.7696 $\pm$ 0.0622	-0.3224 $\pm$ 0.0103	-0.6736 $\pm$ 0.0229	-1.8492 $\pm$ 0.1155	HII
Sb						
KIG56	Sb	-0.7559 $\pm$ 0.0348	-0.3010 $\pm$ 0.0085	-0.5817 $\pm$ 0.0149	-1.7328 $\pm$ 0.0589	HII
KIG187	SABb	1.6055 $\pm$ 0.4364	0.3196 $\pm$ 0.0426	-0.1455 $\pm$ 0.1105	-0.9294 $\pm$ 0.2553	Sy2
KIG204	Sbc	0.5674 $\pm$ 0.1174	0.1586 $\pm$ 0.0394	0.1695 $\pm$ 0.0532	-0.5080 $\pm$ 0.0865	LINER*
KIG208	Sb	-0.3569 $\pm$ 0.1560	-0.4187 $\pm$ 0.0289	-0.3145 $\pm$ 0.0393	-1.6075 $\pm$ 0.2612	HII
KIG211	Sb	0.5423 $\pm$ 0.2881	0.5772 $\pm$ 0.0972	0.3688 $\pm$ 0.1446	-1.0157 $\pm$ 0.8193	S-L $\dagger$
KIG212	SABb	-0.0853 $\pm$ 0.0922	-0.4301 $\pm$ 0.0478	-0.2048 $\pm$ 0.0532	-1.0000 $\pm$ 0.1272	HII
KIG214	Sb	0.9009 $\pm$ 0.0800	-0.4887 $\pm$ 0.0567	-0.4235 $\pm$ 0.0581	-1.2426 $\pm$ 0.0934	Sy1.5
KIG220	Sb	0.4774 $\pm$ 0.5816	0.0746 $\pm$ 0.0781	-0.2010 $\pm$ 0.1732	-1.1532 $\pm$ 0.5865	Sy2
KIG222	SABb	-0.6667 $\pm$ 0.1988	-0.3135 $\pm$ 0.0219	-0.5975 $\pm$ 0.0542	-2.2160 $\pm$ 0.8544	HII
KIG226	Sbc	0.8337 $\pm$ 0.0774	-0.0526 $\pm$ 0.0339	-0.2098 $\pm$ 0.0659	-1.0294 $\pm$ 0.1616	Sy2
KIG238	Sb	-0.7053 $\pm$ 0.0381	-0.3338 $\pm$ 0.0089	-0.6206 $\pm$ 0.0162	-1.8174 $\pm$ 0.0707	HII
KIG242	Sb	0.1977 $\pm$ 0.0211	-0.7730 $\pm$ 0.0188	-0.4173 $\pm$ 0.0191	-1.4277 $\pm$ 0.0582	HII
KIG249	Sbc	-0.2851 $\pm$ 0.0659	-0.5030 $\pm$ 0.0262	-0.2970 $\pm$ 0.0348	-1.4178 $\pm$ 0.1369	HII

Table 6—Continued

Object	M.T. <sup>a</sup>	LOG([O III]/H $\beta$ )	LOG([N II]/H $\alpha$ )	LOG([S II]/H $\alpha$ )	LOG([O I]/H $\alpha$ )	Type
KIG250	SABb	0.2520 $\pm$ 0.0252	-0.5367 $\pm$ 0.0152	-0.3095 $\pm$ 0.0175	-1.0134 $\pm$ 0.0320	HII
KIG252	Sbc	-0.2762 $\pm$ 0.1683	-0.2896 $\pm$ 0.0270	-0.3764 $\pm$ 0.0502	-1.5128 $\pm$ 0.2730	AGN
KIG270	Sbc	-0.3287 $\pm$ 0.0215	-0.3372 $\pm$ 0.0068	-0.5713 $\pm$ 0.0123	-1.7360 $\pm$ 0.0485	HII
KIG274	Sbc	-0.3233 $\pm$ 0.0227	-0.1458 $\pm$ 0.0064	-0.5038 $\pm$ 0.0115	-1.5038 $\pm$ 0.0298	AGN
KIG275	Sbc	-0.2095 $\pm$ 0.2588	-0.1943 $\pm$ 0.0376	-0.5096 $\pm$ 0.1029	-1.4779 $\pm$ 0.4432	AGN
KIG278	SBb	0.4472 $\pm$ 0.0813	-0.1489 $\pm$ 0.0624	0.0039 $\pm$ 0.0784	-0.9399 $\pm$ 0.2305	S-L†
KIG284	Sb	-0.6951 $\pm$ 0.0469	-0.5003 $\pm$ 0.0133	-0.5432 $\pm$ 0.0194	-1.6981 $\pm$ 0.0839	HII
KIG288	Sbc	-0.7337 $\pm$ 0.1083	-0.4823 $\pm$ 0.0206	-0.5405 $\pm$ 0.0409	-1.5252 $\pm$ 0.1363	HII
KIG311	Sbc	-0.6742 $\pm$ 0.0351	-0.4130 $\pm$ 0.0093	-0.5772 $\pm$ 0.0162	-1.6907 $\pm$ 0.0579	HII
KIG318	Sbc	0.5347 $\pm$ 0.7083	-0.1096 $\pm$ 0.0622	-0.3835 $\pm$ 0.1517	-1.1860 $\pm$ 0.3973	Sy2
KIG329	SBbc	0.5302 $\pm$ 0.2424	0.2064 $\pm$ 0.0702	-0.0162 $\pm$ 0.1327	-0.9224 $\pm$ 0.3719	S-L†
KIG333	Sbc	0.1772 $\pm$ 0.3288	-0.1385 $\pm$ 0.0752	-0.4639 $\pm$ 0.2067	-1.2180 $\pm$ 0.5029	AGN
KIG336	Sbc	-0.3357 $\pm$ 0.0250	-0.3257 $\pm$ 0.0105	-0.6850 $\pm$ 0.0208	-1.6651 $\pm$ 0.0658	HII*
KIG339	SBb	-0.6792 $\pm$ 0.0285	-0.3253 $\pm$ 0.0070	-0.6463 $\pm$ 0.0123	-1.7276 $\pm$ 0.0545	HII
KIG340	Sb	-0.2186 $\pm$ 0.1314	-0.3560 $\pm$ 0.0248	-0.4696 $\pm$ 0.0476	-1.4898 $\pm$ 0.1825	HII
KIG344	SBbc	-0.4169 $\pm$ 0.1361	-0.3762 $\pm$ 0.0350	-0.3059 $\pm$ 0.0546	-1.4624 $\pm$ 0.3040	HII
KIG356	Sb	-0.2596 $\pm$ 0.0378	-0.5304 $\pm$ 0.0188	-0.3174 $\pm$ 0.0230	-1.5083 $\pm$ 0.0991	HII
KIG364	Sb	-0.5493 $\pm$ 0.0279	-0.3674 $\pm$ 0.0079	-0.5175 $\pm$ 0.0130	-1.7447 $\pm$ 0.0538	HII
KIG366	SBb	-0.5647 $\pm$ 0.0526	-0.3177 $\pm$ 0.0100	-0.6205 $\pm$ 0.0223	-1.8340 $\pm$ 0.1178	HII
KIG372	Sb	-0.5201 $\pm$ 0.1946	-0.3069 $\pm$ 0.0221	-0.5438 $\pm$ 0.0483	-1.7394 $\pm$ 0.2948	HII
KIG375	Sb	0.7428 $\pm$ 0.7061	0.0497 $\pm$ 0.0597	-0.0861 $\pm$ 0.1054	-1.0066 $\pm$ 0.3168	S-L†
KIG381	Sbc	0.6149 $\pm$ 0.2660	0.6296 $\pm$ 0.1128	0.3971 $\pm$ 0.1658	-0.3771 $\pm$ 0.2953	LINER
KIG392	Sbc	0.3348 $\pm$ 0.1306	0.3275 $\pm$ 0.0466	0.2675 $\pm$ 0.0660	-0.4700 $\pm$ 0.1158	LINER
KIG401	SBbc	0.3140 $\pm$ 0.0744	-0.1632 $\pm$ 0.0206	-0.4415 $\pm$ 0.0486	-1.3965 $\pm$ 0.1591	AGN
KIG409	Sbc	-0.4652 $\pm$ 0.0483	-0.4932 $\pm$ 0.0147	-0.4599 $\pm$ 0.0216	-1.6408 $\pm$ 0.0949	HII

Table 6—Continued

Object	M.T. <sup>a</sup>	LOG([O III]/H $\beta$ )	LOG([N II]/H $\alpha$ )	LOG([S II]/H $\alpha$ )	LOG([O I]/H $\alpha$ )	Type
KIG411	Sbc	-0.0965 $\pm$ 0.2583	-0.0994 $\pm$ 0.0566	-0.3848 $\pm$ 0.1436	-	AGN
KIG414	Sb	0.4089 $\pm$ 0.0815	-0.2854 $\pm$ 0.0323	-0.4811 $\pm$ 0.0687	-1.1393 $\pm$ 0.1334	Sy2
KIG416	Sbc	-0.0035 $\pm$ 0.0237	-0.6216 $\pm$ 0.0137	-0.4171 $\pm$ 0.0161	-1.5132 $\pm$ 0.0595	HII
KIG417	Sbc	-0.7014 $\pm$ 0.3008	-0.3908 $\pm$ 0.0365	-0.8276 $\pm$ 0.1388	-1.5380 $\pm$ 0.3208	HII
KIG418	Sb	-0.4979 $\pm$ 0.0525	-0.4424 $\pm$ 0.0141	-0.4539 $\pm$ 0.0230	-1.4771 $\pm$ 0.0745	HII
KIG419	Sb	-0.2301 $\pm$ 0.0718	-0.2639 $\pm$ 0.0207	-0.5163 $\pm$ 0.0468	-1.5582 $\pm$ 0.2150	AGN
KIG427	Sbc	-0.2588 $\pm$ 0.0969	-0.1719 $\pm$ 0.0221	-0.4055 $\pm$ 0.0489	-1.1845 $\pm$ 0.1088	AGN
KIG430	Sbc	-0.5050 $\pm$ 0.0699	-0.2389 $\pm$ 0.0148	-0.3164 $\pm$ 0.0232	-1.2753 $\pm$ 0.0690	AGN
KIG450	Sb	-0.5942 $\pm$ 0.0750	-0.4627 $\pm$ 0.0172	-0.4417 $\pm$ 0.0260	-1.5650 $\pm$ 0.1121	HII
KIG451	Sb	-0.5078 $\pm$ 0.3730	-0.3353 $\pm$ 0.0555	-0.3692 $\pm$ 0.0997	-1.0835 $\pm$ 0.2247	HII
KIG457	Sbc	-0.2455 $\pm$ 0.0855	-0.2619 $\pm$ 0.0187	-0.2974 $\pm$ 0.0299	-1.1537 $\pm$ 0.0723	AGN
KIG458	Sbc	-0.6233 $\pm$ 0.1419	-0.3485 $\pm$ 0.0320	-0.4470 $\pm$ 0.0553	-1.3634 $\pm$ 0.1758	HII
KIG459	Sb	-0.6314 $\pm$ 0.0646	-0.5119 $\pm$ 0.0160	-0.4322 $\pm$ 0.0231	-1.5847 $\pm$ 0.0999	HII
KIG478	SABb	0.9666 $\pm$ 0.0553	0.1210 $\pm$ 0.0209	-0.1885 $\pm$ 0.0411	-0.9420 $\pm$ 0.0846	Sy2
KIG482	SABb	-0.6511 $\pm$ 0.3409	-0.3357 $\pm$ 0.0404	-0.4804 $\pm$ 0.0872	-1.2983 $\pm$ 0.2823	HII
KIG492	Sbc	0.3795 $\pm$ 0.1389	0.0537 $\pm$ 0.0361	-0.0790 $\pm$ 0.0629	-0.9022 $\pm$ 0.1503	S-L†
KIG493	Sb	-0.4810 $\pm$ 0.1741	-0.3907 $\pm$ 0.0302	-0.6328 $\pm$ 0.0742	-1.2148 $\pm$ 0.1249	HII
KIG497	Sb	-0.1938 $\pm$ 0.2375	-0.2924 $\pm$ 0.0457	-0.3791 $\pm$ 0.0916	-1.1761 $\pm$ 0.2208	AGN
KIG499	SBb	1.3071 $\pm$ 0.0608	0.0680 $\pm$ 0.0245	0.3363 $\pm$ 0.0253	-0.8398 $\pm$ 0.0850	Sy2
KIG507	Sbc	-0.2549 $\pm$ 0.1119	-0.5063 $\pm$ 0.0321	-0.2508 $\pm$ 0.0385	-1.3137 $\pm$ 0.1492	HII
KIG508	SBbc	-0.2771 $\pm$ 0.0096	-0.4934 $\pm$ 0.0064	-0.6521 $\pm$ 0.0100	-1.9427 $\pm$ 0.0348	HII
KIG510	Sbc	-0.3310 $\pm$ 0.0878	-0.3774 $\pm$ 0.0244	-0.3850 $\pm$ 0.0427	-1.4373 $\pm$ 0.1662	HII
KIG515	Sb	-0.6491 $\pm$ 0.0964	-0.4443 $\pm$ 0.0170	-0.5844 $\pm$ 0.0342	-1.6011 $\pm$ 0.1212	HII
KIG516	Sb	-0.4099 $\pm$ 0.0935	-0.4174 $\pm$ 0.0238	-0.3979 $\pm$ 0.0386	-1.3665 $\pm$ 0.1224	HII
KIG522	Sb	-0.4912 $\pm$ 0.0194	-0.2656 $\pm$ 0.0070	-0.6237 $\pm$ 0.0126	-1.8270 $\pm$ 0.0513	AGN

Table 6—Continued

Object	M.T. <sup>a</sup>	LOG([O III]/H $\beta$ )	LOG([N II]/H $\alpha$ )	LOG([S II]/H $\alpha$ )	LOG([O I]/H $\alpha$ )	Type
KIG525	SBb	$-0.3920 \pm 0.0297$	$-0.2504 \pm 0.0100$	$-0.4911 \pm 0.0183$	$-1.5030 \pm 0.0568$	AGN
KIG532	SBb	$-0.4238 \pm 0.0209$	$-0.5065 \pm 0.0092$	$-0.5153 \pm 0.0128$	$-1.7892 \pm 0.0529$	HII
KIG537	Sb	$-0.6258 \pm 0.0272$	$-0.2873 \pm 0.0070$	$-0.5099 \pm 0.0118$	$-1.6709 \pm 0.0473$	HII
KIG541	SABb	$-0.5613 \pm 0.2814$	$-0.3372 \pm 0.0313$	$-0.3167 \pm 0.0555$	$-1.3202 \pm 0.1954$	HII
KIG542	Sb	$-0.7254 \pm 0.0482$	$-0.4622 \pm 0.0106$	$-0.5439 \pm 0.0165$	$-1.7508 \pm 0.0812$	HII
KIG550	SBbc	$0.0492 \pm 0.1287$	$0.2926 \pm 0.0769$	$0.0666 \pm 0.1361$	$-0.9538 \pm 0.4619$	S-L $\dagger$
KIG552	Sb	$-0.3372 \pm 0.0988$	$-0.3234 \pm 0.0158$	$-0.6095 \pm 0.0381$	$-1.4857 \pm 0.1138$	HII
KIG553	SBb	$-0.6341 \pm 0.0470$	$-0.1210 \pm 0.0103$	$-0.6719 \pm 0.0257$	$-1.7644 \pm 0.1089$	AGN*
KIG554	Sb	$-0.6433 \pm 0.2744$	$-0.3176 \pm 0.0274$	$-0.6375 \pm 0.0755$	$-1.3360 \pm 0.1605$	HII
KIG558	Sbc	$-0.0983 \pm 0.0804$	$-0.3517 \pm 0.0251$	$-0.5904 \pm 0.0580$	$-1.4666 \pm 0.1748$	AGN
KIG561	SBbc	$0.9821 \pm 0.1325$	$0.0696 \pm 0.0412$	$-0.1530 \pm 0.0829$	$-0.6976 \pm 0.1191$	LINER
KIG567	SABb	$-0.8176 \pm 0.0883$	$-0.3979 \pm 0.0156$	$-0.6844 \pm 0.0368$	$-1.7377 \pm 0.1414$	HII
KIG575	SABb	$0.3158 \pm 0.0141$	$-0.2156 \pm 0.0092$	$-0.5143 \pm 0.0157$	$-1.1820 \pm 0.0254$	AGN
KIG576	Sb	$0.3784 \pm 0.1310$	$-0.0164 \pm 0.0468$	$-0.2118 \pm 0.0982$	$-1.3500 \pm 0.4741$	S-L $\dagger$
KIG580	Sbc	$-0.7180 \pm 0.0711$	$-0.4235 \pm 0.0132$	$-0.5683 \pm 0.0268$	$-1.7593 \pm 0.1270$	HII
KIG589	Sb	$-0.4432 \pm 0.0644$	$-0.3243 \pm 0.0151$	$-0.5893 \pm 0.0352$	$-1.6566 \pm 0.1669$	HII
KIG593	Sbc	$0.4926 \pm 0.0960$	$0.0763 \pm 0.0371$	$0.0106 \pm 0.0583$	$-0.7684 \pm 0.1207$	S-L $\dagger$
KIG601	Sb	$0.8555 \pm 1.9465$	$0.1053 \pm 0.1438$	$0.0279 \pm 0.2509$	$-1.2635 \pm 1.5425$	AGN
KIG606	SBbc	$-0.2529 \pm 0.1221$	$-0.3989 \pm 0.0285$	$-0.8009 \pm 0.0968$	$-1.5779 \pm 0.2567$	HII
KIG607	Sb	$-0.1921 \pm 0.5565$	$0.0147 \pm 0.1427$	$0.0456 \pm 0.2145$	$-0.7858 \pm 0.5420$	LINER
KIG608	Sbc	$0.2680 \pm 0.6143$	$0.1017 \pm 0.0924$	$-0.3117 \pm 0.2570$	$-0.7202 \pm 0.3178$	S-L $\dagger$
KIG611	Sb	$-0.7421 \pm 0.1384$	$-0.4178 \pm 0.0172$	$-0.7155 \pm 0.0461$	$-1.7411 \pm 0.1895$	HII
KIG612	SBb	$0.4939 \pm 0.0292$	$0.2430 \pm 0.0145$	$0.1860 \pm 0.0197$	$-0.5487 \pm 0.0329$	LINER
KIG613	Sbc	$-0.0437 \pm 0.3242$	$-0.2024 \pm 0.0552$	$-0.3327 \pm 0.1131$	$-1.2601 \pm 0.3653$	AGN
KIG618	Sb	$-0.4638 \pm 0.0265$	$-0.2434 \pm 0.0068$	$-0.4148 \pm 0.0111$	$-1.3825 \pm 0.0306$	AGN



Table 6—Continued

Object	M.T. <sup>a</sup>	LOG([O III]/H $\beta$ )	LOG([N II]/H $\alpha$ )	LOG([S II]/H $\alpha$ )	LOG([O I]/H $\alpha$ )	Type
KIG619	Sbc	-0.2723 $\pm$ 0.0341	-0.5084 $\pm$ 0.0150	-0.3835 $\pm$ 0.0203	-1.4994 $\pm$ 0.0737	HII
KIG628	Sbc	-0.4301 $\pm$ 0.1310	-0.3787 $\pm$ 0.0274	-0.4404 $\pm$ 0.0490	-1.9469 $\pm$ 0.5660	HII
KIG630	Sb	-0.2663 $\pm$ 0.1469	-0.2334 $\pm$ 0.0291	-0.3971 $\pm$ 0.0605	-2.2022 $\pm$ 1.4310	AGN
KIG631	Sb	-0.5954 $\pm$ 0.0440	-0.4219 $\pm$ 0.0137	-0.5790 $\pm$ 0.0242	-1.7948 $\pm$ 0.1268	HII
KIG635	Sbc	-0.0605 $\pm$ 0.0426	-0.6351 $\pm$ 0.0247	-0.3359 $\pm$ 0.0265	-1.2262 $\pm$ 0.0670	HII
KIG640	Sbc	-0.7829 $\pm$ 0.0424	-0.4855 $\pm$ 0.0104	-0.6181 $\pm$ 0.0168	-1.7104 $\pm$ 0.0603	HII
KIG645	Sb	-1.0284 $\pm$ 0.0775	-0.5262 $\pm$ 0.0113	-0.6688 $\pm$ 0.0190	-1.9445 $\pm$ 0.1173	HII
KIG650	Sb	-0.4851 $\pm$ 0.1467	-0.3629 $\pm$ 0.0247	-0.6360 $\pm$ 0.0642	-1.5272 $\pm$ 0.1993	HII
KIG653	Sb	0.5015 $\pm$ 0.1314	0.1930 $\pm$ 0.0415	0.0018 $\pm$ 0.0741	-0.7381 $\pm$ 0.1466	S-L $\dagger$
KIG667	Sb	1.2609 $\pm$ 1.3490	0.2107 $\pm$ 0.0908	-0.0127 $\pm$ 0.1776	-0.9536 $\pm$ 0.5456	Sy2
KIG675	SBb	0.1830 $\pm$ 0.0679	0.0000 $\pm$ 0.0267	-0.0510 $\pm$ 0.0412	-0.8440 $\pm$ 0.0877	LINER
KIG676	Sb	0.0938 $\pm$ 0.1327	-0.2581 $\pm$ 0.0388	-0.1549 $\pm$ 0.0559	-1.0458 $\pm$ 0.1425	LINER
KIG719	SBb	-0.4437 $\pm$ 0.0076	-0.6990 $\pm$ 0.0066	-1.1832 $\pm$ 0.0172	-1.8900 $\pm$ 0.0297	HII*
KIG723	SBb	-0.3979 $\pm$ 0.1915	-0.3445 $\pm$ 0.0376	-0.5461 $\pm$ 0.0883	-1.6775 $\pm$ 0.4815	HII
KIG725	Sb	-0.7979 $\pm$ 0.0363	-0.4168 $\pm$ 0.0091	-0.6624 $\pm$ 0.0154	-1.7119 $\pm$ 0.0506	HII
KIG731	Sb	-0.5917 $\pm$ 0.0991	-0.3672 $\pm$ 0.0162	-0.5294 $\pm$ 0.0313	-1.7035 $\pm$ 0.1618	HII
KIG739	Sbc	-0.5110 $\pm$ 0.0384	-0.4791 $\pm$ 0.0121	-0.5153 $\pm$ 0.0195	-1.6923 $\pm$ 0.0892	HII
KIG743	Sb	-0.4183 $\pm$ 0.0469	-0.2722 $\pm$ 0.0116	-0.3680 $\pm$ 0.0186	-1.4667 $\pm$ 0.0659	AGN
KIG749	Sbc	0.7515 $\pm$ 0.0216	-0.0310 $\pm$ 0.0124	-0.0610 $\pm$ 0.0169	-0.7634 $\pm$ 0.0281	Sy1.8
KIG752	Sb	-0.5832 $\pm$ 0.0921	-0.3512 $\pm$ 0.0171	-0.5556 $\pm$ 0.0323	-1.7687 $\pm$ 0.1733	HII
KIG757	Sb	0.6113 $\pm$ 0.0429	-0.1168 $\pm$ 0.0220	-0.4439 $\pm$ 0.0550	-1.3613 $\pm$ 0.1694	Sy2
KIG762	Sbc	0.8411 $\pm$ 0.3795	0.3430 $\pm$ 0.0535	0.2583 $\pm$ 0.0781	-0.6873 $\pm$ 0.1914	S-L $\dagger$
KIG767	Sb	0.7086 $\pm$ 0.5268	0.2822 $\pm$ 0.0986	-0.3372 $\pm$ 0.3500	-0.5859 $\pm$ 0.3153	Sy2
KIG780	Sb	1.0785 $\pm$ 0.2355	0.1658 $\pm$ 0.0320	-0.3241 $\pm$ 0.0877	-1.2505 $\pm$ 0.2828	Sy2
KIG795	Sb	-0.0775 $\pm$ 0.0938	-0.1820 $\pm$ 0.0127	-0.3554 $\pm$ 0.0250	-1.3358 $\pm$ 0.0877	AGN

Table 6—Continued

Object	M.T. <sup>a</sup>	LOG([O III]/H $\beta$ )	LOG([N II]/H $\alpha$ )	LOG([S II]/H $\alpha$ )	LOG([O I]/H $\alpha$ )	Type
KIG807	Sbc	$-0.7275 \pm 0.1407$	$-0.2921 \pm 0.0155$	$-0.5002 \pm 0.0338$	$-1.3789 \pm 0.0926$	HII
KIG884	Sbc	$-0.0912 \pm 0.2233$	$-0.2999 \pm 0.0316$	$-0.4766 \pm 0.0711$	$-1.4094 \pm 0.2327$	AGN
KIG892	Sbc	$-0.6198 \pm 0.2338$	$-0.3832 \pm 0.0255$	$-0.7560 \pm 0.0794$	$-2.3737 \pm 1.3022$	HII
KIG907	Sbc	$-0.1022 \pm 0.0932$	$-0.5283 \pm 0.0413$	$-0.2481 \pm 0.0506$	$-1.1883 \pm 0.1483$	HII
KIG912	Sb	$-0.7228 \pm 0.0731$	$-0.4308 \pm 0.0142$	$-0.5156 \pm 0.0240$	$-1.6445 \pm 0.1000$	HII
KIG923	Sb	$-0.3809 \pm 0.0710$	$-0.3515 \pm 0.0144$	$-0.4158 \pm 0.0242$	$-1.8544 \pm 0.1882$	HII
KIG931	Sbc	$-0.9289 \pm 0.0778$	$-0.4692 \pm 0.0102$	$-0.5506 \pm 0.0178$	$-1.7904 \pm 0.1032$	HII
KIG943	Sb	$-0.6898 \pm 0.0272$	$-0.3556 \pm 0.0073$	$-0.6048 \pm 0.0130$	$-1.7271 \pm 0.0505$	HII
KIG1008	SBb	$1.1463 \pm 0.0465$	$0.1739 \pm 0.0240$	$-0.0825 \pm 0.0394$	$-0.6212 \pm 0.0535$	Sy1.5
Sc						
KIG198	SABc	$-0.3940 \pm 0.1875$	$-0.4120 \pm 0.0263$	$-0.7347 \pm 0.0794$	$-1.6353 \pm 0.2751$	HII
KIG199	Sc	$-0.6611 \pm 0.0956$	$-0.4273 \pm 0.0161$	$-0.5352 \pm 0.0288$	$-1.8179 \pm 0.1902$	HII
KIG203	SABc	$-0.8569 \pm 0.4712$	$-0.3949 \pm 0.0360$	$-0.4559 \pm 0.0736$	$-1.1814 \pm 0.1748$	HII
KIG216	Sc	$-0.4758 \pm 0.2365$	$-0.3753 \pm 0.0286$	$-0.5737 \pm 0.0708$	$-1.5198 \pm 0.2344$	HII
KIG217	Sc	$-0.9164 \pm 0.0545$	$-0.4944 \pm 0.0104$	$-0.6484 \pm 0.0170$	$-1.8422 \pm 0.0775$	HII
KIG221	Sc	$-0.3468 \pm 0.0891$	$-0.2996 \pm 0.0227$	$-0.5924 \pm 0.0574$	$-1.7947 \pm 0.3442$	AGN
KIG225	Sc	$-0.6280 \pm 0.3485$	$-0.2305 \pm 0.0479$	$-0.5263 \pm 0.1293$	$-1.4466 \pm 0.4868$	AGN
KIG229	Sc	$-0.4510 \pm 0.1911$	$-0.3274 \pm 0.0364$	$-0.3878 \pm 0.0633$	$-1.1301 \pm 0.1601$	HII
KIG241	Sc	$-0.3639 \pm 0.0452$	$-0.4714 \pm 0.0159$	$-0.4442 \pm 0.0231$	$-1.7636 \pm 0.1450$	HII
KIG248	Sc	$1.0423 \pm 0.0081$	$-0.0423 \pm 0.0050$	$-0.2417 \pm 0.0074$	$-0.8813 \pm 0.0103$	Sy2
KIG254	Sc	$-0.9208 \pm 0.1033$	$-0.4021 \pm 0.0145$	$-0.6721 \pm 0.0301$	$-1.8473 \pm 0.1582$	HII
KIG260	Sc	$-0.3859 \pm 0.1531$	$-0.4424 \pm 0.0362$	$-0.5610 \pm 0.0756$	$-2.1611 \pm 1.1609$	HII
KIG263	Sc	$0.7272 \pm 0.5186$	$0.2105 \pm 0.0822$	$0.1284 \pm 0.1218$	$-0.8566 \pm 0.3604$	S-L†
KIG268	SABc	$-0.3799 \pm 0.2076$	$-0.4847 \pm 0.0603$	$-0.3298 \pm 0.0775$	$-1.7922 \pm 0.7811$	HII

Table 6—Continued

Object	M.T. <sup>a</sup>	LOG([O III]/H $\beta$ )	LOG([N II]/H $\alpha$ )	LOG([S II]/H $\alpha$ )	LOG([O I]/H $\alpha$ )	Type
KIG271	Sc	$-0.5853 \pm 0.2039$	$-0.3401 \pm 0.0302$	$-0.5427 \pm 0.0723$	$-1.6380 \pm 0.3510$	HII
KIG273	Sc	$-0.9066 \pm 0.0568$	$-0.2990 \pm 0.0081$	$-0.6857 \pm 0.0166$	$-1.8872 \pm 0.0824$	HII
KIG282	Sc	$-0.2090 \pm 0.1574$	$-0.2501 \pm 0.0223$	$-0.4277 \pm 0.0465$	$-1.3762 \pm 0.1526$	AGN
KIG289	Sc	$0.2165 \pm 0.1065$	$-0.1635 \pm 0.0310$	$-0.4142 \pm 0.0706$	$-1.6038 \pm 0.4342$	AGN
KIG291	Scd	$-0.3190 \pm 0.0405$	$-0.5553 \pm 0.0163$	$-0.3600 \pm 0.0188$	$-1.5727 \pm 0.1107$	HII
KIG294	Sc	$-0.0073 \pm 0.1698$	$-0.4654 \pm 0.0435$	$-0.3224 \pm 0.0611$	$-1.2101 \pm 0.1705$	HII
KIG296	Sc	$-0.7204 \pm 0.1316$	$-0.3901 \pm 0.0229$	$-0.4451 \pm 0.0405$	$-1.6912 \pm 0.2496$	HII
KIG300	Sc	$0.3790 \pm 0.0177$	$-1.0948 \pm 0.0249$	$-0.4973 \pm 0.0179$	$-1.4475 \pm 0.0537$	HII
KIG306	Sc	$-0.3548 \pm 0.0927$	$-0.4394 \pm 0.0216$	$-0.3509 \pm 0.0322$	$-1.8250 \pm 0.3316$	HII
KIG307	Sc	$0.2462 \pm 0.2639$	$-0.0352 \pm 0.0545$	$-0.1816 \pm 0.1061$	$-1.3388 \pm 0.5529$	S-L†
KIG308	Sc	$-0.0462 \pm 0.3078$	$-0.1372 \pm 0.0655$	$-0.3954 \pm 0.1609$	$-1.6338 \pm 1.0450$	AGN
KIG314	SABc	$-0.2541 \pm 0.0447$	$-0.3206 \pm 0.0214$	$-0.6235 \pm 0.0496$	$-2.2972 \pm 0.8334$	AGN
KIG321	Sc	$-0.2127 \pm 0.0666$	$-0.5433 \pm 0.0232$	$-0.3566 \pm 0.0318$	$-1.2098 \pm 0.0829$	HII
KIG322	Sc	$-0.4786 \pm 0.0661$	$-0.3720 \pm 0.0187$	$-0.4091 \pm 0.0296$	$-1.7492 \pm 0.2186$	HII
KIG323	Sc	$-0.3838 \pm 0.1108$	$-0.3308 \pm 0.0206$	$-0.5184 \pm 0.0445$	$-1.4326 \pm 0.1359$	HII
KIG326	SBC	$-0.0369 \pm 0.1847$	$-0.3616 \pm 0.0622$	$-0.0756 \pm 0.0633$	$-1.0533 \pm 0.2470$	LINER
KIG328	SABc	$-0.3110 \pm 0.0915$	$-0.2665 \pm 0.0270$	$-0.4153 \pm 0.0560$	$-1.4968 \pm 0.2389$	AGN
KIG330	Sc	$-0.4832 \pm 0.1200$	$-0.37037 \pm 0.0271$	$-0.4190 \pm 0.0487$	$-1.6139 \pm 0.2766$	AGN
KIG337	Sc	$0.7518 \pm 0.2335$	$0.0899 \pm 0.0408$	$-0.2396 \pm 0.0924$	$-1.1599 \pm 0.2894$	Sy2
KIG343	SBC	$-0.8360 \pm 0.0828$	$-0.4859 \pm 0.0131$	$-0.5192 \pm 0.0228$	$-1.8243 \pm 0.1539$	HII
KIG348	Sc	$0.1154 \pm 0.0140$	$-0.6746 \pm 0.0117$	$-0.4785 \pm 0.0137$	$-1.4493 \pm 0.0346$	HII
KIG353	Sc	$-0.6722 \pm 0.0411$	$-0.5039 \pm 0.0108$	$-0.5129 \pm 0.0168$	$-1.6810 \pm 0.0809$	HII
KIG360	Sc	$-0.3699 \pm 0.0424$	$-0.4564 \pm 0.0152$	$-0.4383 \pm 0.0219$	$-1.4498 \pm 0.0754$	HII
KIG362	Sc	$0.2775 \pm 0.0680$	$0.1049 \pm 0.0231$	$0.0840 \pm 0.0345$	$-0.7344 \pm 0.0732$	LINER
KIG365	Sc	$-0.5798 \pm 0.0236$	$-0.4098 \pm 0.0086$	$-0.5431 \pm 0.0131$	$-1.9773 \pm 0.0759$	HII

Table 6—Continued

Object	M.T. <sup>a</sup>	LOG([O III]/H $\beta$ )	LOG([N II]/H $\alpha$ )	LOG([S II]/H $\alpha$ )	LOG([O I]/H $\alpha$ )	Type
KIG367	SABc	-0.5025 $\pm$ 0.1428	-0.4254 $\pm$ 0.0280	-0.3999 $\pm$ 0.0475	-1.7043 $\pm$ 0.3366	HII
KIG368	Sc	-0.9190 $\pm$ 0.1051	-0.3950 $\pm$ 0.0134	-0.6971 $\pm$ 0.0313	-1.6126 $\pm$ 0.0915	HII
KIG370	Sc	-0.8182 $\pm$ 0.0797	-0.4485 $\pm$ 0.0113	-0.7419 $\pm$ 0.0255	-2.1264 $\pm$ 0.2139	HII
KIG373	Sc	-0.8433 $\pm$ 0.1244	-0.3724 $\pm$ 0.0155	-0.5514 $\pm$ 0.0334	-1.6996 $\pm$ 0.1577	HII
KIG384	Sc	-0.3252 $\pm$ 0.1262	-0.4385 $\pm$ 0.0326	-0.5818 $\pm$ 0.0607	-1.8999 $\pm$ 0.5140	HII
KIG386	Sc	-0.4308 $\pm$ 0.0822	-0.2396 $\pm$ 0.0165	-0.3974 $\pm$ 0.0310	-1.6777 $\pm$ 0.1898	AGN
KIG391	Sc	0.2374 $\pm$ 0.0526	-0.6375 $\pm$ 0.0399	-0.2390 $\pm$ 0.0373	-1.2277 $\pm$ 0.1169	HII
KIG395	Sc	0.4926 $\pm$ 0.0955	0.4213 $\pm$ 0.0544	0.1874 $\pm$ 0.0895	-0.4904 $\pm$ 0.1469	LINER
KIG398	Sc	-0.4113 $\pm$ 0.1728	-0.3639 $\pm$ 0.0338	-0.5659 $\pm$ 0.0761	-2.2222 $\pm$ 1.2918	HII
KIG399	SBC	-0.4976 $\pm$ 0.0659	-0.4616 $\pm$ 0.0154	-0.7162 $\pm$ 0.0349	-1.6450 $\pm$ 0.1091	HII
KIG403	Sc	0.0416 $\pm$ 0.3936	-0.1835 $\pm$ 0.0611	-0.3110 $\pm$ 0.1202	-1.0981 $\pm$ 0.3055	LINER
KIG405	SABc	-0.7206 $\pm$ 0.0882	-0.4599 $\pm$ 0.0160	-0.4800 $\pm$ 0.0264	-1.6434 $\pm$ 0.1172	HII
KIG406	Sc	-0.6869 $\pm$ 0.0745	-0.4215 $\pm$ 0.0140	-0.5105 $\pm$ 0.0239	-1.7292 $\pm$ 0.1210	HII
KIG407	Sc	0.5809 $\pm$ 0.0136	-1.2032 $\pm$ 0.0243	-0.6533 $\pm$ 0.0175	-1.6662 $\pm$ 0.0608	HII
KIG408	Sc	-0.5202 $\pm$ 0.0842	-0.4492 $\pm$ 0.0215	-0.3755 $\pm$ 0.0336	-1.4595 $\pm$ 0.1372	HII
KIG410	Sc	-0.1348 $\pm$ 0.0090	-0.4794 $\pm$ 0.0057	-0.5713 $\pm$ 0.0081	-1.7658 $\pm$ 0.0233	HII
KIG428	SBC	0.6087 $\pm$ 0.5510	-0.3683 $\pm$ 0.0997	-0.0313 $\pm$ 0.0959	-0.8327 $\pm$ 0.2308	S-L†
KIG429	Sc	0.1542 $\pm$ 0.4310	-0.1788 $\pm$ 0.0547	-0.4304 $\pm$ 0.1336	-	AGN
KIG432	Scd	0.0021 $\pm$ 0.1392	0.1091 $\pm$ 0.1830	0.0797 $\pm$ 0.2714	-1.1747 $\pm$ 1.5783	LINER
KIG436	SBC	-0.6726 $\pm$ 0.0526	-0.4329 $\pm$ 0.0128	-0.4914 $\pm$ 0.0218	-1.6115 $\pm$ 0.0901	HII
KIG440	Sc	1.1854 $\pm$ 1.3201	0.1239 $\pm$ 0.0561	-0.5199 $\pm$ 0.2369	-0.7619 $\pm$ 0.1950	Sy2
KIG442	SBC	-0.0942 $\pm$ 0.0620	-0.4464 $\pm$ 0.0278	-0.1781 $\pm$ 0.0291	-1.3940 $\pm$ 0.1487	HII
KIG445	Sc	-0.8403 $\pm$ 0.2002	-0.4075 $\pm$ 0.0226	-0.6364 $\pm$ 0.0525	-1.4098 $\pm$ 0.1257	HII
KIG446	SBC	-0.7051 $\pm$ 0.1581	-0.4457 $\pm$ 0.0236	-0.8129 $\pm$ 0.0745	-2.0652 $\pm$ 0.5377	HII
KIG448	SABc	-0.9581 $\pm$ 0.0194	-0.4005 $\pm$ 0.0050	-0.7380 $\pm$ 0.0086	-2.1090 $\pm$ 0.0423	HII

Table 6—Continued

Object	M.T. <sup>a</sup>	LOG([O III]/H $\beta$ )	LOG([N II]/H $\alpha$ )	LOG([S II]/H $\alpha$ )	LOG([O I]/H $\alpha$ )	Type
KIG453	Sc	-0.1938 $\pm$ 0.1556	-0.2848 $\pm$ 0.0285	-0.5543 $\pm$ 0.0751	-1.5441 $\pm$ 0.2815	AGN
KIG454	Sc	-0.6045 $\pm$ 0.1290	-0.3909 $\pm$ 0.0235	-0.5985 $\pm$ 0.0580	-1.4907 $\pm$ 0.1867	HII
KIG473	SABc	-0.2148 $\pm$ 0.1502	-0.3366 $\pm$ 0.0414	-0.2623 $\pm$ 0.0717	-1.0582 $\pm$ 0.1504	AGN
KIG474	Sc	-0.0374 $\pm$ 0.0356	-0.6191 $\pm$ 0.0199	-0.3771 $\pm$ 0.0249	-1.4477 $\pm$ 0.0902	HII
KIG476	Scd	0.0824 $\pm$ 0.0315	-0.7432 $\pm$ 0.0227	-0.4151 $\pm$ 0.0232	-1.5135 $\pm$ 0.0979	HII
KIG477	Sc	0.4178 $\pm$ 0.0238	-0.1635 $\pm$ 0.0131	-0.4579 $\pm$ 0.0262	-1.3465 $\pm$ 0.0689	Sy2
KIG486	Sc	0.3076 $\pm$ 0.0550	-1.0042 $\pm$ 0.0781	-0.4722 $\pm$ 0.0546	-1.5040 $\pm$ 0.2361	HII
KIG487	SBcd	0.3345 $\pm$ 0.0096	-0.8796 $\pm$ 0.0098	-0.5919 $\pm$ 0.0110	-1.6670 $\pm$ 0.0368	HII
KIG498	Sc	-0.5868 $\pm$ 0.0204	-0.3058 $\pm$ 0.0058	-0.4559 $\pm$ 0.0089	-1.6054 $\pm$ 0.0298	HII
KIG502	SABc	0.2796 $\pm$ 0.0177	-0.8653 $\pm$ 0.0181	-0.5028 $\pm$ 0.0173	-1.5729 $\pm$ 0.0772	HII
KIG509	SABc	-0.2996 $\pm$ 0.0674	-0.4489 $\pm$ 0.0231	-0.3198 $\pm$ 0.0286	-1.5614 $\pm$ 0.1650	HII
KIG512	Sc	-0.5086 $\pm$ 0.0938	-0.4669 $\pm$ 0.0221	-0.4237 $\pm$ 0.0326	-2.0899 $\pm$ 0.5159	HII
KIG518	SABc	-0.8838 $\pm$ 0.5779	-0.3348 $\pm$ 0.0326	-0.4637 $\pm$ 0.0621	-1.7497 $\pm$ 0.4449	HII
KIG524	Scd	-0.0691 $\pm$ 0.0266	-0.7193 $\pm$ 0.0177	-0.3002 $\pm$ 0.0165	-1.2848 $\pm$ 0.0581	HII
KIG526	Sc	-0.3985 $\pm$ 0.0720	-0.3299 $\pm$ 0.0145	-0.4979 $\pm$ 0.0283	-1.4314 $\pm$ 0.1058	HII
KIG546	Sc	-0.6198 $\pm$ 0.2869	-0.3236 $\pm$ 0.0362	-0.5079 $\pm$ 0.0826	-1.6534 $\pm$ 0.4771	HII
KIG547	SABc	-0.5136 $\pm$ 0.1139	-0.5091 $\pm$ 0.0360	-0.2687 $\pm$ 0.0392	-1.6509 $\pm$ 0.3420	HII
KIG551	SABc	0.4260 $\pm$ 0.1333	-0.5306 $\pm$ 0.0721	-0.1670 $\pm$ 0.0669	-0.8214 $\pm$ 0.1310	AGN
KIG560	Sc	0.0687 $\pm$ 0.0174	-0.6555 $\pm$ 0.0133	-0.3778 $\pm$ 0.0153	-1.3371 $\pm$ 0.0391	HII
KIG563	Sc	-0.4012 $\pm$ 0.0388	-0.4000 $\pm$ 0.0138	-0.4471 $\pm$ 0.0213	-1.6111 $\pm$ 0.1091	HII
KIG565	Sc	-0.2981 $\pm$ 0.1312	-0.3181 $\pm$ 0.0291	-0.4666 $\pm$ 0.0599	-1.4309 $\pm$ 0.2196	AGN
KIG566	Sc	0.3478 $\pm$ 0.0204	-1.0096 $\pm$ 0.0252	-0.5568 $\pm$ 0.0215	-1.6160 $\pm$ 0.0985	HII
KIG568	Sc	0.1594 $\pm$ 0.7950	0.2174 $\pm$ 0.1064	-0.0430 $\pm$ 0.2185	-0.7412 $\pm$ 0.4141	LINER
KIG583	Sc	-0.5283 $\pm$ 0.1807	-0.3930 $\pm$ 0.0289	-0.5853 $\pm$ 0.0690	-1.4791 $\pm$ 0.2142	HII
KIG590	Sc	-0.2762 $\pm$ 0.0154	-0.6464 $\pm$ 0.0109	-0.4731 $\pm$ 0.0126	-1.7940 $\pm$ 0.0546	HII

Table 6—Continued

Object	M.T. <sup>a</sup>	LOG([O III]/H $\beta$ )	LOG([N II]/H $\alpha$ )	LOG([S II]/H $\alpha$ )	LOG([O I]/H $\alpha$ )	Type
KIG594	Sc	-0.4446 $\pm$ 0.0383	-0.4484 $\pm$ 0.0131	-0.5147 $\pm$ 0.0204	-1.6548 $\pm$ 0.0858	HII
KIG598	Sc	-0.3378 $\pm$ 0.0838	-0.3797 $\pm$ 0.0299	-0.6079 $\pm$ 0.0777	-1.7806 $\pm$ 0.4383	HII
KIG600	Scd	-0.1721 $\pm$ 0.1535	-0.4560 $\pm$ 0.0451	-0.2436 $\pm$ 0.0567	-1.3257 $\pm$ 0.2327	HII
KIG603	Sc	0.1781 $\pm$ 0.1156	0.0483 $\pm$ 0.0230	0.1587 $\pm$ 0.0296	-0.4901 $\pm$ 0.0441	LINER*
KIG610	SABc	-0.5699 $\pm$ 0.0431	-0.3919 $\pm$ 0.0123	-0.5891 $\pm$ 0.0219	-1.6704 $\pm$ 0.0834	HII
KIG625	Sc	-0.5398 $\pm$ 0.0882	-0.3936 $\pm$ 0.0160	-0.4439 $\pm$ 0.0266	-1.5243 $\pm$ 0.1095	HII
KIG626	SABc	-0.4974 $\pm$ 0.0399	-0.4910 $\pm$ 0.0120	-0.5275 $\pm$ 0.0179	-1.7206 $\pm$ 0.0883	HII
KIG639	Sc	-0.4978 $\pm$ 0.1549	-0.3795 $\pm$ 0.0260	-0.4834 $\pm$ 0.0523	-1.9841 $\pm$ 0.5599	HII
KIG648	Sc	-0.5528 $\pm$ 0.1171	-0.4117 $\pm$ 0.0227	-0.6253 $\pm$ 0.0535	-1.7270 $\pm$ 0.2531	HII
KIG651	SBC	0.2553 $\pm$ 0.0128	-0.7991 $\pm$ 0.0125	-0.4875 $\pm$ 0.0131	-1.5145 $\pm$ 0.0377	HII
KIG652	Sc	-0.5891 $\pm$ 0.0536	-0.4092 $\pm$ 0.0123	-0.4716 $\pm$ 0.0189	-1.5628 $\pm$ 0.0685	HII
KIG655	Sc	-0.4754 $\pm$ 0.7579	-0.0501 $\pm$ 0.0851	-0.2672 $\pm$ 0.1892	-0.9730 $\pm$ 0.4011	AGN
KIG659	Sc	-0.5086 $\pm$ 0.1769	-0.4156 $\pm$ 0.0355	-0.4631 $\pm$ 0.0664	-1.2537 $\pm$ 0.1656	HII
KIG668	Sc	-0.3766 $\pm$ 0.1273	-0.4480 $\pm$ 0.0238	-0.4281 $\pm$ 0.0385	-1.4956 $\pm$ 0.1523	HII
KIG672	Sc	0.0713 $\pm$ 0.1848	-0.2318 $\pm$ 0.0400	-0.3023 $\pm$ 0.0777	-1.4365 $\pm$ 0.3575	AGN
KIG680	Sc	-0.1041 $\pm$ 0.2175	-0.2030 $\pm$ 0.0427	-0.6550 $\pm$ 0.1577	-1.0325 $\pm$ 0.1763	AGN
KIG681	Scd	-0.1487 $\pm$ 0.1917	-0.3696 $\pm$ 0.0461	-0.4068 $\pm$ 0.0716	-1.2545 $\pm$ 0.2159	AGN
KIG683	Sc	-0.5643 $\pm$ 0.1252	-0.4190 $\pm$ 0.0167	-0.6486 $\pm$ 0.0370	-2.3988 $\pm$ 0.7433	HII
KIG688	Sc	-0.5421 $\pm$ 0.1242	-0.3741 $\pm$ 0.0209	-0.5427 $\pm$ 0.0473	-1.5691 $\pm$ 0.1894	HII
KIG691	SBCd	-0.3228 $\pm$ 0.0792	-0.4572 $\pm$ 0.0199	-0.3316 $\pm$ 0.0245	-1.7552 $\pm$ 0.2404	HII
KIG693	Sc	-0.7150 $\pm$ 0.1728	-0.4271 $\pm$ 0.0252	-0.6320 $\pm$ 0.0624	-1.7152 $\pm$ 0.3057	HII
KIG700	Scd	-0.1759 $\pm$ 0.1425	-0.3546 $\pm$ 0.0480	-0.2215 $\pm$ 0.0650	-1.3888 $\pm$ 0.3886	AGN
KIG709	Sc	0.4863 $\pm$ 1.4057	-0.1015 $\pm$ 0.0432	-0.4466 $\pm$ 0.1154	-1.2837 $\pm$ 0.3242	Sy2
KIG716	Sc	0.2789 $\pm$ 0.1337	0.2548 $\pm$ 0.0703	0.1630 $\pm$ 0.1071	-0.5213 $\pm$ 0.1833	LINER
KIG717	Sc	-0.5746 $\pm$ 0.1918	-0.4114 $\pm$ 0.0233	-0.5526 $\pm$ 0.0504	-2.2380 $\pm$ 0.7953	HII

Table 6—Continued

Object	M.T. <sup>a</sup>	LOG([O III]/H $\beta$ )	LOG([N II]/H $\alpha$ )	LOG([S II]/H $\alpha$ )	LOG([O I]/H $\alpha$ )	Type
KIG721	Sc	$-0.6518 \pm 0.0890$	$-0.4415 \pm 0.0192$	$-0.6844 \pm 0.0434$	$-1.8561 \pm 0.2447$	HII
KIG744	Sc	$0.0489 \pm 0.1837$	$-0.3825 \pm 0.0435$	$-0.1585 \pm 0.0501$	$-0.9633 \pm 0.1311$	LINER
KIG747	Sc	$0.3158 \pm 0.0220$	$-0.1517 \pm 0.0113$	$-0.5229 \pm 0.0218$	$-1.2944 \pm 0.0449$	Sy1.5
KIG748	SBC	$0.3615 \pm 0.0513$	$-0.7205 \pm 0.0475$	$-0.3451 \pm 0.0416$	$-1.4186 \pm 0.1837$	HII
KIG754	Scd	$-0.5846 \pm 0.0988$	$-0.4161 \pm 0.0227$	$-0.4729 \pm 0.0429$	$-1.4281 \pm 0.1281$	HII
KIG902	Sc	$-0.8253 \pm 0.1299$	$-0.4449 \pm 0.0157$	$-0.6600 \pm 0.0335$	$-1.8632 \pm 0.1846$	HII
KIG928	Sc	$-0.5977 \pm 0.0492$	$-0.4458 \pm 0.0132$	$-0.5908 \pm 0.0241$	$-1.7567 \pm 0.1068$	HII
KIG980	Sc	$-0.1461 \pm 0.0250$	$-0.5747 \pm 0.0126$	$-0.4733 \pm 0.0173$	$-1.5829 \pm 0.0594$	HII
KIG1030	SBC	$-0.1305 \pm 0.0487$	$-0.6196 \pm 0.0234$	$-0.3989 \pm 0.0275$	$-1.6204 \pm 0.1619$	HII
KIG1041	Sc	$-0.1243 \pm 0.1771$	$-0.3244 \pm 0.0445$	$-0.1947 \pm 0.0624$	$-1.4422 \pm 0.4265$	AGN
Sm						
KIG280	Sm	$-0.1951 \pm 0.2746$	$-0.3680 \pm 0.0673$	$-0.1298 \pm 0.0855$	$-1.7026 \pm 1.0415$	HII
KIG283	Irr	$0.0976 \pm 0.0322$	$-0.7516 \pm 0.0221$	$-0.3673 \pm 0.0212$	$-1.5913 \pm 0.1111$	HII
KIG290	SABd	$0.0000 \pm 0.0889$	$-0.7892 \pm 0.0750$	$-0.2253 \pm 0.0491$	$-1.4944 \pm 0.3311$	HII
KIG299	SBm	$0.2350 \pm 0.0485$	$-0.8851 \pm 0.0514$	$-0.4300 \pm 0.0388$	$-1.1289 \pm 0.0936$	HII
KIG313	Sd	$0.0000 \pm 0.1697$	$-0.2189 \pm 0.0413$	$-0.6978 \pm 0.1489$	$-1.8633 \pm 0.8821$	AGN
KIG354	Sm	$0.0804 \pm 0.1385$	$-0.5136 \pm 0.0403$	$-0.2366 \pm 0.0435$	$-1.3186 \pm 0.2033$	HII
KIG355	Irr	$-0.5558 \pm 0.0238$	$-0.4612 \pm 0.0083$	$-0.4600 \pm 0.0115$	$-1.6367 \pm 0.0398$	HII
KIG439	Sdm	$-0.1691 \pm 0.0500$	$-0.5207 \pm 0.0190$	$-0.4420 \pm 0.0304$	$-1.5046 \pm 0.1151$	HII
KIG447	Irr	$0.2305 \pm 0.0094$	$-0.9002 \pm 0.0092$	$-0.6691 \pm 0.0103$	$-1.8389 \pm 0.0306$	HII
KIG470	Irr	$0.2109 \pm 0.0266$	$-0.9434 \pm 0.0333$	$-0.4939 \pm 0.0258$	$-1.4647 \pm 0.0958$	HII
KIG536	Sd	$0.4303 \pm 0.0316$	$-1.0425 \pm 0.0533$	$-0.5223 \pm 0.0359$	$-1.4192 \pm 0.1088$	HII
KIG569	Sd	$0.3600 \pm 0.0102$	$-1.0040 \pm 0.0117$	$-0.6116 \pm 0.0112$	$-1.6435 \pm 0.0368$	HII
KIG584	Irr	$0.0670 \pm 0.2626$	$-0.7595 \pm 0.2265$	$-0.1912 \pm 0.1350$	$-0.9828 \pm 0.3666$	HII
KIG585	Sd	$-0.3652 \pm 0.0654$	$-0.5155 \pm 0.0180$	$-0.4048 \pm 0.0260$	$-1.4033 \pm 0.0786$	HII

Table 6—Continued

Object	M.T. <sup>a</sup>	LOG([O III]/H $\beta$ )	LOG([N II]/H $\alpha$ )	LOG([S II]/H $\alpha$ )	LOG([O I]/H $\alpha$ )	Type
KIG642	SABd	$0.0637 \pm 0.0291$	$-0.7332 \pm 0.0219$	$-0.4192 \pm 0.0225$	$-1.2843 \pm 0.0633$	HII
KIG662	SBd	$0.6521 \pm 0.0102$	$-1.3676 \pm 0.0185$	$-0.8652 \pm 0.0144$	$-1.9460 \pm 0.0502$	HII
KIG674	Sm	$0.6314 \pm 0.3125$	$-0.1586 \pm 0.0617$	$-0.4863 \pm 0.2035$	$-1.0995 \pm 0.3442$	Sy2
KIG909	Sdm	$-0.7043 \pm 0.2292$	$-0.4137 \pm 0.0259$	$-0.6653 \pm 0.0651$	$-1.7201 \pm 0.2953$	HII
KIG937	SBd	$-0.2003 \pm 0.2570$	$-0.3921 \pm 0.1261$	$0.0288 \pm 0.1193$	$-1.0904 \pm 0.5402$	HII
KIG990	IAB	$0.6726 \pm 0.0081$	$-1.3646 \pm 0.0135$	$-0.9131 \pm 0.0124$	$-1.9868 \pm 0.0420$	HII

<sup>a</sup>M.T.- Morphological Type. AGN classification denotes those galaxies that are AGN according to the [N II] diagrams but not to the [S II] and/or [O I].

<sup>†</sup>L-S classification means that galaxies fall in the separation line for Seyfert and LINER according to [S II] and [O I] diagrams.

\*Type with weak broad component in permitted lines. Seyfert quantitative classification according to Winkler (1992).



Table 7. Logarithm intensities ratios and their errors for the Varela’s sample. Labels like on Table 6.

Object	M.T. <sup>a</sup>	LOG([O III]/H $\beta$ )	LOG([N II]/H $\alpha$ )	LOG([S II]/H $\alpha$ )	LOG([O I]/H $\alpha$ )	Type
Elliptical						
PGC29177	E-SO	-0.0385 $\pm$ 0.0075	-0.4953 $\pm$ 0.0064	-0.6389 $\pm$ 0.0090	-1.9657 $\pm$ 0.0284	HII
PGC36037	E-SO	0.6757 $\pm$ 0.2136	-0.0778 $\pm$ 0.0767	-0.0145 $\pm$ 0.1076	-0.8049 $\pm$ 0.2415	S-L†
PGC36211	E	0.1761 $\pm$ 0.0310	-0.5803 $\pm$ 0.0225	-0.2478 $\pm$ 0.0225	-1.3349 $\pm$ 0.0808	HII
PGC43121	E-SO	0.4754 $\pm$ 0.0048	-0.9475 $\pm$ 0.0054	-0.8785 $\pm$ 0.0066	-1.9157 $\pm$ 0.0141	HII
Spheroidal						
PGC25467	S0-a	-0.4046 $\pm$ 0.0283	-0.3493 $\pm$ 0.0119	-0.4011 $\pm$ 0.0177	-1.5501 $\pm$ 0.0721	HII
PGC28259	S0	0.5808 $\pm$ 0.0168	-0.4437 $\pm$ 0.0169	-0.2733 $\pm$ 0.0206	-0.8945 $\pm$ 0.0330	Sy2
PGC28758	S0-a	0.7331 $\pm$ 0.0062	-1.2866 $\pm$ 0.0097	-1.0391 $\pm$ 0.0110	-2.0580 $\pm$ 0.0283	HII
PGC31601	S0	0.2531 $\pm$ 0.0109	-0.5715 $\pm$ 0.0092	-0.6821 $\pm$ 0.0158	-1.4981 $\pm$ 0.0367	HII
PGC31945	S0	0.3114 $\pm$ 0.0078	-0.7400 $\pm$ 0.0077	-0.6240 $\pm$ 0.0094	-1.7853 $\pm$ 0.0261	HII
PGC37574	S0	0.5721 $\pm$ 0.1763	0.1109 $\pm$ 0.0813	0.3262 $\pm$ 0.0894	-0.7749 $\pm$ 0.2968	S-L†
PGC37795	S0	0.2274 $\pm$ 0.0869	-0.1798 $\pm$ 0.0652	-0.0085 $\pm$ 0.0795	-0.6710 $\pm$ 0.1398	LINER
PGC38527	S0-a	-0.5243 $\pm$ 0.1138	-0.3784 $\pm$ 0.0264	-0.6363 $\pm$ 0.0662	-1.8257 $\pm$ 0.4031	HII
PGC39681	S0-a	-0.4022 $\pm$ 0.0433	-0.5761 $\pm$ 0.0196	-0.5402 $\pm$ 0.0273	-1.9586 $\pm$ 0.2593	HII
PGC42497	S0	-0.6131 $\pm$ 0.0237	-0.5466 $\pm$ 0.0088	-0.6258 $\pm$ 0.0124	-2.0000 $\pm$ 0.0691	HII
PGC49927	S0-a	-0.0588 $\pm$ 0.0085	-0.5192 $\pm$ 0.0064	-0.6233 $\pm$ 0.0088	-2.0442 $\pm$ 0.0365	HII
PGC49956	S0-a	0.8751 $\pm$ 0.2953	0.3010 $\pm$ 0.0670	0.1846 $\pm$ 0.1030	-0.8093 $\pm$ 0.3120	S-L†
PGC58183	S0	0.8329 $\pm$ 0.2360	0.3401 $\pm$ 0.0796	0.2683 $\pm$ 0.1140	-0.4705 $\pm$ 0.2014	LINER
PGC48521	S0	1.0883 $\pm$ 0.0117	0.0723 $\pm$ 0.0076	-0.3273 $\pm$ 0.0143	-0.8754 $\pm$ 0.0190	Sy1.8
Sa						
PGC25985	SBa	0.0186 $\pm$ 0.0498	-0.6120 $\pm$ 0.0328	-0.1932 $\pm$ 0.0294	-1.1732 $\pm$ 0.0948	HII
PGC26218	Sa	-0.0440 $\pm$ 0.0097	-0.6207 $\pm$ 0.0068	-0.6754 $\pm$ 0.0092	-2.0514 $\pm$ 0.0384	HII
PGC27437	Sa	0.4566 $\pm$ 0.1065	0.2900 $\pm$ 0.0494	0.0912 $\pm$ 0.0839	-0.5104 $\pm$ 0.1302	LINER
PGC28145	Sa	-0.6816 $\pm$ 0.0373	-0.2678 $\pm$ 0.0078	-0.5870 $\pm$ 0.0139	-1.7602 $\pm$ 0.0546	HII

Table 7—Continued

Object	M.T. <sup>a</sup>	LOG([O III]/H $\beta$ )	LOG([N II]/H $\alpha$ )	LOG([S II]/H $\alpha$ )	LOG([O I]/H $\alpha$ )	Type
PGC38582	Sab	-0.8523 $\pm$ 0.0308	-0.5166 $\pm$ 0.0088	-0.5855 $\pm$ 0.0121	-2.0038 $\pm$ 0.0636	HII
PGC40475	Sa	-0.1320 $\pm$ 0.0143	-0.4863 $\pm$ 0.0092	-0.5244 $\pm$ 0.0128	-1.6922 $\pm$ 0.0437	HII
PGC42174	SABa	-0.1253 $\pm$ 0.0601	0.0771 $\pm$ 0.0187	-0.1549 $\pm$ 0.0330	-0.8434 $\pm$ 0.0603	LINER
PGC50198	Sa	-0.5946 $\pm$ 0.0278	-0.4892 $\pm$ 0.0093	-0.5302 $\pm$ 0.0128	-1.7903 $\pm$ 0.0528	HII
PGC50745	SBa	-0.7138 $\pm$ 0.0273	-0.2834 $\pm$ 0.0088	-0.5423 $\pm$ 0.0131	-1.7481 $\pm$ 0.0518	HII
PGC51091	SBa	-0.4356 $\pm$ 0.0259	-0.2945 $\pm$ 0.0094	-0.4890 $\pm$ 0.0156	-1.6721 $\pm$ 0.0641	AGN
PGC51951	Sa	-0.5768 $\pm$ 0.0359	-0.4364 $\pm$ 0.0117	-0.4763 $\pm$ 0.0179	-1.5721 $\pm$ 0.0673	HII
Sb						
PGC26690	SBbc	0.5302 $\pm$ 0.2424	0.2064 $\pm$ 0.0702	0.0142 $\pm$ 0.1266	-0.9224 $\pm$ 0.3719	S-L†
PGC27311	Sbc	0.4115 $\pm$ 0.0075	-1.0317 $\pm$ 0.0092	-0.6730 $\pm$ 0.0092	-1.8906 $\pm$ 0.0278	HII
PGC27518	Sbc	-0.7164 $\pm$ 0.0532	-0.4294 $\pm$ 0.0120	-0.6720 $\pm$ 0.0250	-1.9476 $\pm$ 0.1586	HII
PGC27796	SBb	-0.2766 $\pm$ 0.1091	-0.1786 $\pm$ 0.0197	-0.3907 $\pm$ 0.0388	-1.3352 $\pm$ 0.1223	AGN
PGC29347	SBb	0.3436 $\pm$ 0.0074	-0.8179 $\pm$ 0.0075	-0.6724 $\pm$ 0.0089	-2.0031 $\pm$ 0.0291	HII
PGC29715	SBb	-0.3502 $\pm$ 0.0624	-0.3763 $\pm$ 0.0169	-0.5435 $\pm$ 0.0324	-1.4794 $\pm$ 0.0993	HII
PGC30010	Sb	-0.4184 $\pm$ 0.0298	-0.1828 $\pm$ 0.0091	-0.5548 $\pm$ 0.0181	-1.5933 $\pm$ 0.0621	AGN
PGC35314	Sb	0.4141 $\pm$ 0.0818	0.0241 $\pm$ 0.0312	0.0514 $\pm$ 0.0424	-0.9643 $\pm$ 0.1298	S-L†
PGC37928	Sb	-0.3429 $\pm$ 0.0163	-0.4129 $\pm$ 0.0083	-0.4976 $\pm$ 0.0116	-1.8935 $\pm$ 0.0562	HII
PGC38802	Sb	0.3390 $\pm$ 0.0651	0.1107 $\pm$ 0.0394	0.0181 $\pm$ 0.0619	-1.0505 $\pm$ 0.2307	S-L†
PGC39393	SABb	-0.2865 $\pm$ 0.1896	-0.2614 $\pm$ 0.0361	-0.5564 $\pm$ 0.0931	-1.7686 $\pm$ 0.5994	AGN
PGC43113	Sb	0.7704 $\pm$ 0.2383	-0.0286 $\pm$ 0.0427	0.0749 $\pm$ 0.0548	-0.9961 $\pm$ 0.1968	S-L†
PGC45836	SABb	0.3158 $\pm$ 0.0141	-0.2156 $\pm$ 0.0092	-0.5143 $\pm$ 0.0157	-1.1820 $\pm$ 0.0254	Sy2
PGC47482	SBb	-0.6782 $\pm$ 0.0462	-0.4185 $\pm$ 0.0123	-0.6252 $\pm$ 0.0229	-1.6744 $\pm$ 0.0842	HII
PGC47985	Sb	-0.2839 $\pm$ 0.0417	-0.4473 $\pm$ 0.0161	-0.3025 $\pm$ 0.0196	-1.3910 $\pm$ 0.0678	HII
PGC50889	Sb	-0.2788 $\pm$ 0.0389	-0.1876 $\pm$ 0.0116	-0.3563 $\pm$ 0.0194	-1.3643 $\pm$ 0.0603	AGN
PGC52488	SBb	-0.1362 $\pm$ 0.0362	-0.4720 $\pm$ 0.0174	-0.3628 $\pm$ 0.0235	-1.4771 $\pm$ 0.0946	HII

Table 7—Continued

Object	M.T. <sup>a</sup>	LOG([O III]/H $\beta$ )	LOG([N II]/H $\alpha$ )	LOG([S II]/H $\alpha$ )	LOG([O I]/H $\alpha$ )	Type
PGC52887	Sb	0.6649 $\pm$ 0.0417	-0.0303 $\pm$ 0.0303	-0.2710 $\pm$ 0.0628	-0.7351 $\pm$ 0.0789	Sy2
PGC55419	Sbc	-0.5714 $\pm$ 0.0265	-0.4478 $\pm$ 0.0108	-0.5763 $\pm$ 0.0168	-2.0686 $\pm$ 0.1290	HII
PGC71699	Sbc	-0.5825 $\pm$ 0.0773	-0.3239 $\pm$ 0.0153	-0.4023 $\pm$ 0.0263	-1.5000 $\pm$ 0.1227	HII
PGC8165	Sb	-0.4385 $\pm$ 0.0686	-0.3378 $\pm$ 0.0161	-0.5935 $\pm$ 0.0388	-1.7169 $\pm$ 0.1955	HII
Sc						
PGC2600	SABc	-0.5967 $\pm$ 0.0427	-0.3670 $\pm$ 0.0105	-0.7098 $\pm$ 0.0245	-1.8781 $\pm$ 0.1226	HII
PGC27968	SABc	0.2112 $\pm$ 0.0363	-0.7672 $\pm$ 0.0285	-0.4197 $\pm$ 0.0284	-1.3424 $\pm$ 0.0962	HII
PGC28485	SABc	-0.3216 $\pm$ 0.2285	-0.2406 $\pm$ 0.0381	-0.4330 $\pm$ 0.0828	-2.3499 $\pm$ 2.6570	AGN
PGC30197	Sc	-0.6006 $\pm$ 0.0406	-0.3603 $\pm$ 0.0091	-0.4818 $\pm$ 0.0141	-1.8556 $\pm$ 0.0831	HII
PGC30569	Sc	-0.5203 $\pm$ 0.0579	-0.4690 $\pm$ 0.0151	-0.3830 $\pm$ 0.0206	-1.5418 $\pm$ 0.0964	HII
PGC30858	Sc	0.0000 $\pm$ 0.0367	-0.6320 $\pm$ 0.0272	-0.3158 $\pm$ 0.0273	-1.1761 $\pm$ 0.0759	HII
PGC31883	Sc	0.2561 $\pm$ 0.1406	0.0722 $\pm$ 0.0617	-0.1450 $\pm$ 0.1211	-0.9006 $\pm$ 0.2643	S-L†
PGC32183	SBC	-0.1205 $\pm$ 0.0604	-0.4301 $\pm$ 0.0281	-0.1619 $\pm$ 0.0295	-1.3777 $\pm$ 0.1490	HII
PGC34935	Sc	0.4217 $\pm$ 0.0241	-0.1635 $\pm$ 0.0131	-0.4579 $\pm$ 0.0262	-1.3465 $\pm$ 0.0689	Sy2
PGC36930	Sc	0.1207 $\pm$ 0.0143	-0.8679 $\pm$ 0.0129	-0.5590 $\pm$ 0.0128	-1.7928 $\pm$ 0.0527	HII
PGC37352	SABc	-0.2688 $\pm$ 0.0615	-0.4489 $\pm$ 0.0231	-0.3198 $\pm$ 0.0286	-1.4523 $\pm$ 0.1300	HII
PGC37444	Sc	-0.5434 $\pm$ 0.0918	-0.4669 $\pm$ 0.0221	-0.3840 $\pm$ 0.0304	-2.0899 $\pm$ 0.5159	HII
PGC37584	Scd	-0.3540 $\pm$ 0.0505	-0.5241 $\pm$ 0.0154	-0.4119 $\pm$ 0.0195	-1.6200 $\pm$ 0.1108	HII
PGC37838	Sc	0.4091 $\pm$ 0.0562	-0.8096 $\pm$ 0.0575	-0.3734 $\pm$ 0.0452	-1.0314 $\pm$ 0.0854	HII
PGC38150	SABc	-0.9508 $\pm$ 0.5681	-0.3415 $\pm$ 0.0329	-0.4637 $\pm$ 0.0621	-1.7497 $\pm$ 0.4449	HII
PGC38277	S?	0.3059 $\pm$ 0.0169	-0.9774 $\pm$ 0.0166	-0.5873 $\pm$ 0.0155	-1.8220 $\pm$ 0.0733	HII
PGC38286	Sc	0.3501 $\pm$ 0.0958	-0.8921 $\pm$ 0.0703	-0.3268 $\pm$ 0.0437	-1.1139 $\pm$ 0.1129	HII
PGC44370	Sc	0.1347 $\pm$ 0.0296	-0.6326 $\pm$ 0.0244	-0.3648 $\pm$ 0.0275	-1.5586 $\pm$ 0.1378	HII
PGC44797	SBC	-0.9261 $\pm$ 0.0190	-0.4801 $\pm$ 0.0060	-0.6909 $\pm$ 0.0090	-2.3028 $\pm$ 0.0668	HII
PGC47577	Sc	-0.2762 $\pm$ 0.0154	-0.6306 $\pm$ 0.0110	-0.4573 $\pm$ 0.0127	-1.7782 $\pm$ 0.0547	HII

Table 7—Continued

Object	M.T. <sup>a</sup>	LOG([O III]/H $\beta$ )	LOG([N II]/H $\alpha$ )	LOG([S II]/H $\alpha$ )	LOG([O I]/H $\alpha$ )	Type
PGC48959	SABc	$-0.5680 \pm 0.0566$	$-0.3579 \pm 0.0124$	$-0.3907 \pm 0.0183$	$-1.4153 \pm 0.0603$	HII
PGC49112	SABc	$0.0130 \pm 0.1143$	$-0.1027 \pm 0.0333$	$-0.2990 \pm 0.0666$	$-1.1916 \pm 0.2003$	S-L†
PGC52607	Sc	$-0.9324 \pm 0.0811$	$-0.4480 \pm 0.0138$	$-0.5572 \pm 0.0227$	$-1.9501 \pm 0.1731$	HII
PGC58115	Sc	$-0.7097 \pm 0.0779$	$-0.4992 \pm 0.0163$	$-0.5993 \pm 0.0282$	$-2.1493 \pm 0.3284$	HII
PGC58336	Sc	$-0.1787 \pm 0.2136$	$-0.2606 \pm 0.0475$	$-0.2704 \pm 0.0774$	$-1.0571 \pm 0.2865$	LINER
PGC32543	Scd	$0.3692 \pm 0.0128$	$-0.9844 \pm 0.0184$	$-0.5072 \pm 0.0153$	$-1.6016 \pm 0.0541$	HII
PGC32364	Scd	$0.2784 \pm 0.0155$	$-0.9480 \pm 0.0204$	$-0.4698 \pm 0.0167$	$-1.5613 \pm 0.0571$	HII
Sm						
PGC27792	Sd	$-0.1027 \pm 0.0880$	$-0.4600 \pm 0.0357$	$-0.3258 \pm 0.0469$	$-1.4637 \pm 0.2458$	HII
PGC34967	Sd	$0.1557 \pm 0.0141$	$-0.6801 \pm 0.0101$	$-0.4639 \pm 0.0117$	$-1.5552 \pm 0.0356$	HII
PGC47938	Irr	$0.5449 \pm 0.0121$	$-1.4242 \pm 0.0354$	$-0.7214 \pm 0.0193$	$-1.8103 \pm 0.0771$	HII
PGC27157	Irr	$0.5783 \pm 0.0074$	$-1.2818 \pm 0.0137$	$-0.7089 \pm 0.0107$	$-1.7392 \pm 0.0311$	HII